AEDC-TR-75-73

FLOW GENERATION PROPERTIES OF FIVE TRANSONIC WIND TUNNEL TEST SECTION WALL CONFIGURATIONS

PROPULSION WIND TUNNEL FACILITY
ARNOLD ENGINEERING DEVELOPMENT CENTER
AIR FORCE SYSTEMS COMMAND
ARNOLD AIR FORCE STATION, TENNESSEE 37389

August 1975

Final Report for Period July 1 — December 9, 1974

Prepared for

DIRECTORATE OF TECHNOLOGY
ARNOLD ENGINEERING DEVELOPMENT CENTER
ARNOLD AIR FORCE STATION, TENNESSEE 37389

NOTICES

When U. S. Government drawings specifications, or other data are used for any purpose other than a definitely related Government procurement operation, the Government thereby incurs no responsibility nor any obligation whatsoever, and the fact that the Government may have formulated, furnished, or in any way supplied the said drawings, specifications, or other data, is not to be regarded by implication or otherwise, or in any manner licensing the holder or any other person or corporation, or conveying any rights or permission to manufacture, use, or sell any patented invention that may in any way be related thereto.

Qualified users may obtain copies of this report from the Defense Documentation Center.

References to named commercial products in this report are not to be considered in any sense as an endorsement of the product by the United States Air Force or the Government.

This report has been reviewed by the Information Office (OI) and is releasable to the National Technical Information Service (NTIS). At NTIS, it will be available to the general public, including foreign nations.

APPROVAL STATEMENT

This technical report has been reviewed and is approved for publication.

FOR THE COMMANDER

CARLOS TIRRES
Captain, USAF
Research & Development
Division
Directorate of Technology

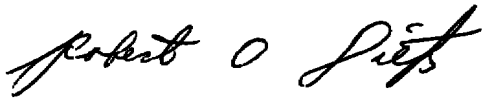

ROBERT O. DIETZ
Director of Technology

REPORT DOCUMENTATION PAGE		READ INSTRUCTIONS BEFORE COMPLETING FORM
1 REPORT NUMBER AEDC-TR-75-73	2 GOVT ACCESSION NO.	3 RECIPIENT'S CATALOG NUMBER
4. TITLE (and Subtitle) FLOW GENERATION PROPERTIES OF FIVE TRANSONIC WIND TUNNEL TEST SECTION WALL CONFIGURATIONS		5 TYPE OF REPORT & PERIOD COVERED Final Report, Jul 1 - Dec 9, 1974 6 PERFORMING ORG. REPORT NUMBER
7 AUTHOR(s) R. L. Parker, Jr., ARO, Inc.		8. CONTRACT OR GRANT NUMBER(s)
9 PERFORMING ORGANIZATION NAME AND ADDRESS Arnold Engineering Development Center (DY) Arnold Air Force Station, TN 37389		10. PROGRAM ELEMENT, PROJECT, TASK AREA & WORK UNIT NUMBERS Program Element 65807F
11. CONTROLLING OFFICE NAME AND ADDRESS Arnold Engineering Development Center (DYFS), Arnold Air Force Station, TN 37389		12. REPORT DATE August 1975 13 NUMBER OF PAGES 46
14 MONITORING AGENCY NAME & ADDRESS(if different from Controlling Office)		15 SECURITY CLASS. (of this report) UNCLASSIFIED 15a. DECLASSIFICATION/DOWNGRADING SCHEDULE N/A

16 DISTRIBUTION STATEMENT (of this Report)

Approved for public release; distribution unlimited.

17 DISTRIBUTION STATEMENT (of the abstract entered in Block 20, if different from Report)

18 SUPPLEMENTARY NOTES

Available in DDC.

19 KEY WORDS (Continue on reverse side if necessary and identify by block number)

wind tunnels
wind tunnel tests
wall effects
porosity
interference
transonic wind tunnels
walls

20 ABSTRACT (Continue on reverse side if necessary and identify by block number)

Tests were conducted in the Aerodynamic Wind Tunnel (1T) of the Propulsion Wind Tunnel Facility to determine the tunnel calibration and centerline Mach number distribution for five transonic wall configurations. Data were also obtained with a cone-cylinder model to determine the effects of model blockage on the free-stream Mach number development in the test section. During the test, the Mach number was varied from 0.6 to 1.3. The wall

DD FORM 1 JAN 73 1473 EDITION OF 1 NOV 65 IS OBSOLETE

20, Continued

porosity was varied to obtain data at representative values for each wall configuration. This report presents the test results and provides data to guide the operation of Tunnel 1T with the five transonic wall configurations.

AFSC
Arnold AFS Tenn

PREFACE

The work reported herein was conducted by the Arnold Engineering Development Center (AEDC), Air Force Systems Command (AFSC), Arnold Air Force Station, Tennessee, under Program Element 65807F. The results were obtained by ARO, Inc. (a subsidiary of Sverdrup & Parcel and Associates, Inc.), contract operator of AEDC, AFSC, Arnold Air Force Station, Tennessee, under ARO Project Number P32A-29A. The author of this technical report was R. L. Parker, Jr., ARO, Inc. The manuscript (ARO Control No. ARO-PWT-TR-75-37) was submitted for publication on March 26, 1975.

CONTENTS

ILLUSTRATIONS

Figure

Figure Page

TABLES

1.0 INTRODUCTION

Recent data (Refs. 1 and 2, for example) have shown that present wind tunnel perforated wall configurations generate interference in the high subsonic Mach number range. The model pressure field and shock locations are modified because of improper wall characteristics when moderate to large regions of local supercritical flow exist about the model. Also, as yet unpublished data obtained in the Propulsion Wind Tunnel Facility (PWT) Aerodynamic Wind Tunnel (1T) with a 2-percent blockage cone-cylinder model and data obtained in the PWT Aerodynamic Wind Tunnel (4T) with a 1-percent blockage cone-cylinder model (Ref. 2) provide evidence that the model may affect the test section Mach number in a sense opposite to classical blockage effects.

A program has been initiated at AEDC to develop improved wall concepts that reduce the effects of noise, turbulence, and wall interference on test data from transonic wind tunnels. Assessment of the wall performance is to be based on the properties of flow generation, noise generation, supercritical flow interference, and wave attenuation. The results of the flow generation tests on five transonic wall configurations are presented in this report.

Tunnel calibration and centerline Mach number distribution were determined for each configuration using a centerline static probe. The effect of the model on the tunnel calibration Mach number was determined by comparing the Mach number distribution in the nozzle with and without a cone-cylinder model mounted concentric with the centerline static probe. In addition, data were obtained to indicate if truncation of the test section by the diffuser adversely affects the return of the model-perturbed flow to free-stream conditions.

2.0 APPARATUS

2.1 TEST FACILITY

Tunnel 1T is a continuous flow, nonreturn wind tunnel equipped with a two-dimensional, flexible nozzle and an auxiliary plenum evacuation system. The tunnel may be operated in the Mach number range from 0.2 to 1.5. Supersonic nozzle contours are used to generate Mach numbers above 1.15. The tunnel is operated at a total pressure of approximately 2850 psfa, depending on the tunnel resistance and ambient atmospheric conditions. The stagnation temperature can be varied from 80 to 120°F above ambient temperature, as necessary to prevent visible condensation from occurring in the test section. The general arrangement of the tunnel is shown in Fig. 1.

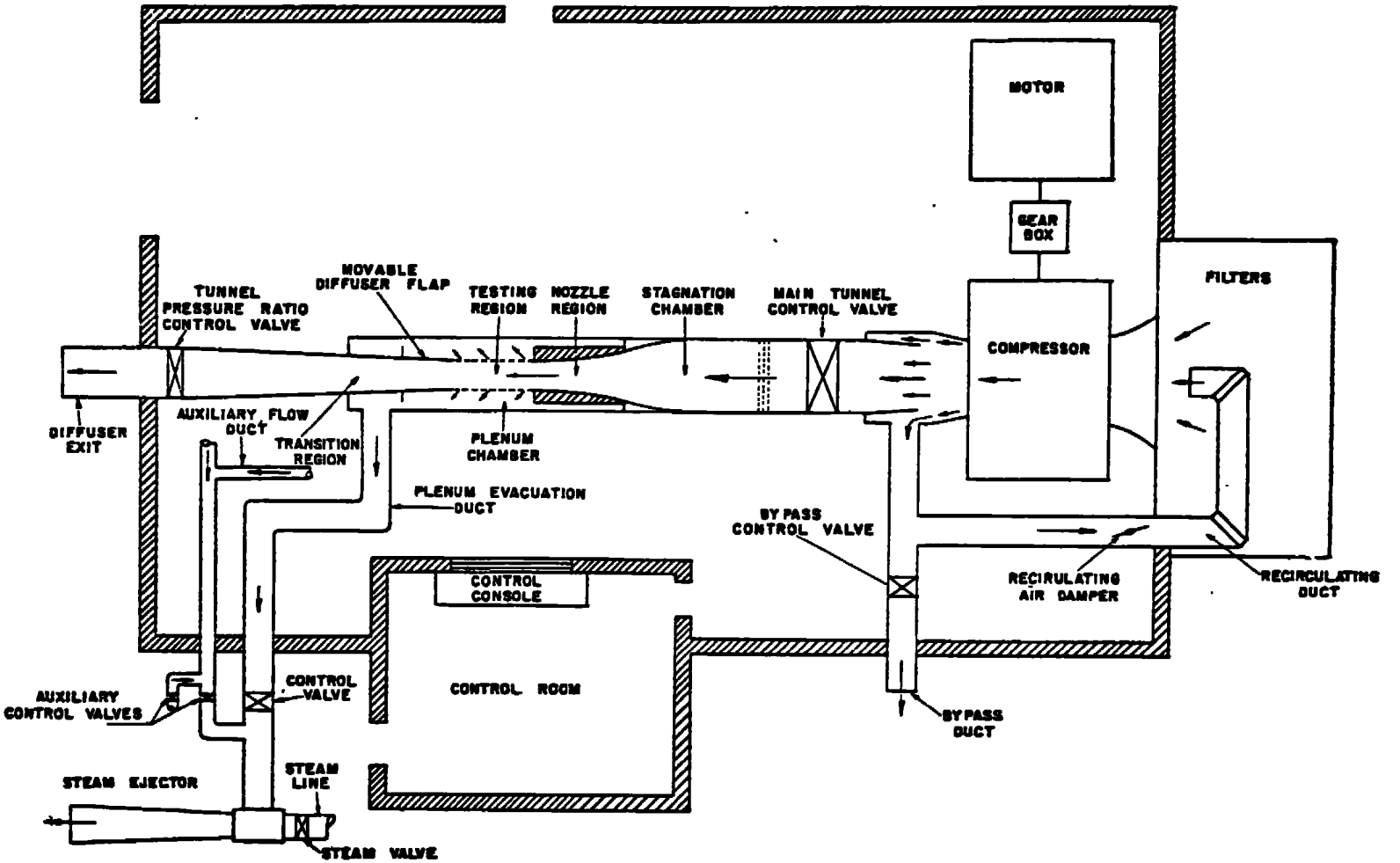

Figure 1. General arrangement of Tunnel 1T and supporting equipment.

The test section, composed of four removable walls, is 37.5 in. in length and 12 in. square at its entrance. The top and bottom walls are supported by flexures at the nozzle exit and by remotely actuated screwjacks at the downstream end to allow variations in wall angle. The side walls are parallel and are not adjustable.

2.2 WALL CONFIGURATIONS

2.2.1 Low-Aspect-Ratio-Hole Wall (LAR)

It is indicated in Ref. 3 that a perforated wall with a small ratio of plate thickness to hole diameter may produce linear crossflow characteristics. The LAR wall incorporates the low-aspect-ratio hole design along with a variable porosity feature. The wall consists of a liner and cutoff plate each 0.125 in. thick with 0.213-in.-diam holes inclined to the airstream at an angle of 60 deg (see Fig. 2 for wall hole pattern). The holes are equally spaced in rows 0.713 in. apart. Wall porosity can be varied from 2 to 7 percent by displacing the cutoff plate either upstream or downstream. Figure 3 shows the variation of porosity with cutoff plate displacement.

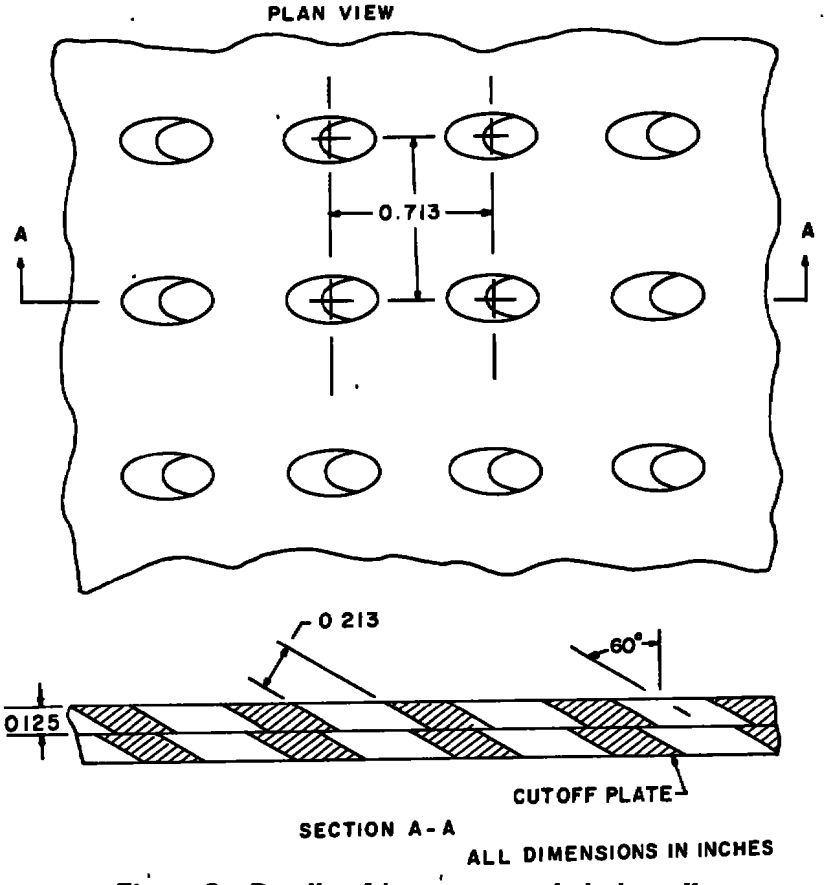

Figure 2. Details of low-aspect-ratio-hole wall.

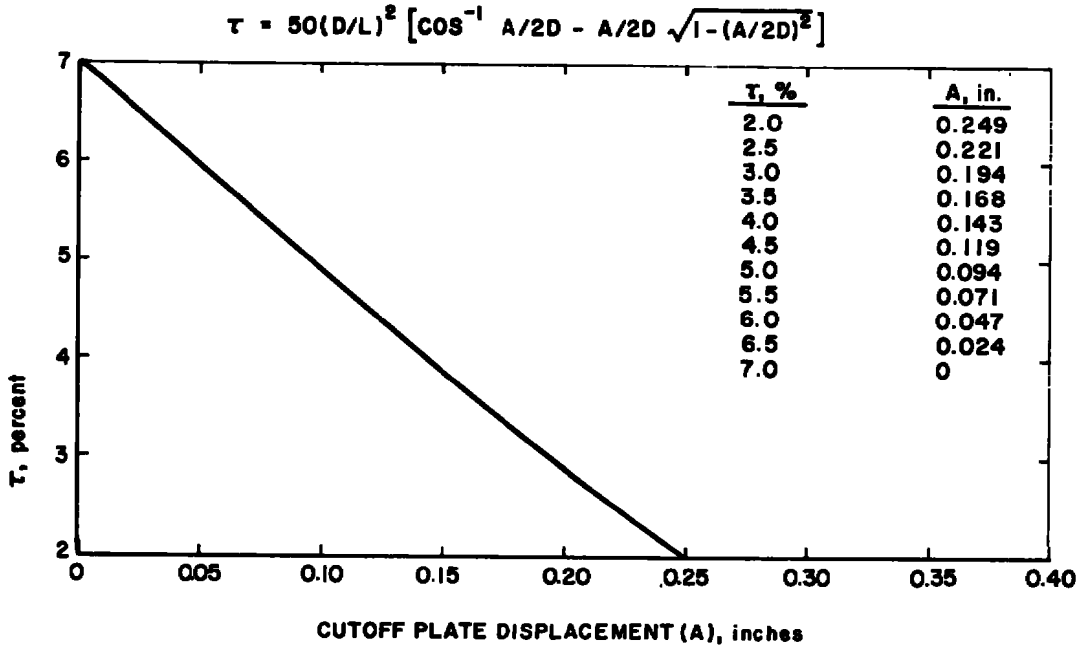

Figure 3. Variation of porosity with cutoff plate displacement, LAR wall.

2.2.2 Axially Distributed Porosity Perforated Wall (ADP)

Consideration of a lifting wing model in a rectangular wind tunnel has led to the determination of a theoretical distribution of wall porosity for zero upwash interference. A relationship derived from the subsonic field equation and the classical perforated wall boundary factor ($R = 2\theta/C_P$) is given by

$$R/\beta = \frac{\left[\left(\frac{x}{b\beta}\right)^2 + \lambda^2\right]^{3/2} + \left(\frac{x}{b\beta}\right)^3 + 2\left(\frac{x}{b\beta}\right)\lambda^2}{\lambda} \qquad (1)$$

where x is the tunnel station measured from the 0.25 chord of the model. The porosity distribution was found by combining Eq. (1) with the porosity parameter,

$$Q = (1 + \beta/R)^{-1} \qquad (2)$$

Values of Q = 0 and 1 correspond to solid and open walls, respectively. Reference 4 shows that a value of Q = 0.6 corresponds to 5-percent porosity for the variable porosity wall of Tunnel 4T. A functional relationship between Q and τ was found by applying a least-squares polynominal curve fit to an arbitrary monotonic curve faired through the values of Q = 0, 0.6, and 1.0 and τ = 0, 5, and 10 percent, respectively. Although the

distribution of R/β given by Eq. (1) is a function of Mach number, the variation with Mach number is small. The distribution representing M = 0.8 was chosen as the basis for the ADP wall porosity distribution.

The Tunnel 1T variable porosity wall, Fig. 4, is geometrically similar to the Tunnel 4T wall. The top and bottom variable porosity walls were modified to achieve the desired distribution of porosity by filling the necessary holes with putty. Cutoff plate displacement (see Fig. 4) provides an overall porosity adjustment. It should be noted that in Eq. (1) R/β becomes negative, which has no physical meaning, for values of x less than that corresponding to tunnel station 14. Between stations 2 and 14 the porosity is set at 15 percent of the maximum porosity to allow for smooth Mach number development. Figure 5 shows the resulting ADP wall porosity distribution for several maximum wall porosity

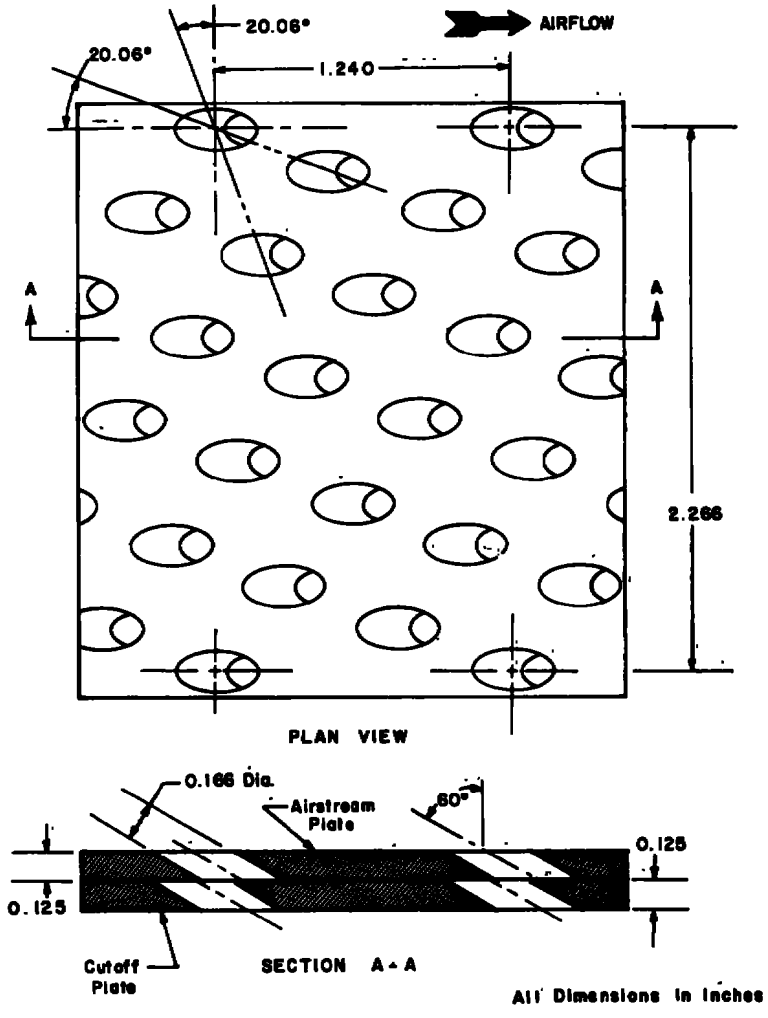

Figure 4. Details of variable porosity wall.

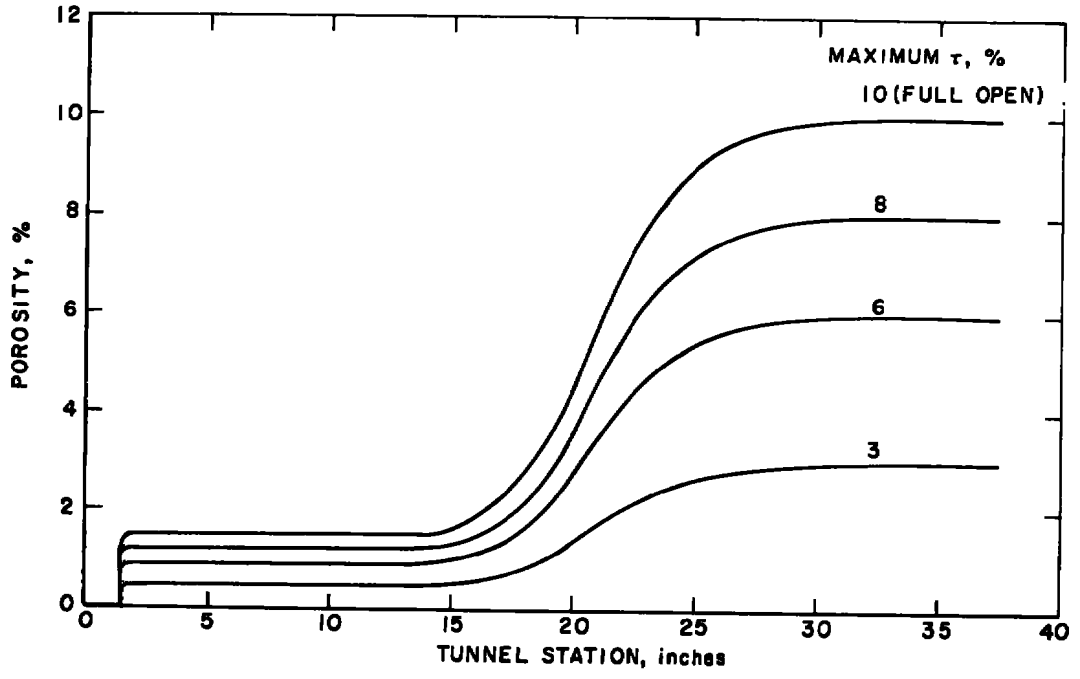

Figure 5. Axial porosity distribution, ADP wall.

settings. For convenience, the wall porosity for the ADP wall is designated by the maximum value, which occurs downstream of tunnel station 32. The side walls were set at a constant, uniform 5-percent porosity regardless of the top and bottom wall porosity setting.

2.2.3 Modified Rod Wall (2R)

The 2R wall configuration consists of solid side walls with ventilated top and bottom walls, the latter being manufactured by assembling 0.25-in.-diam polished stainless steel rods parallel to the tunnel axis as shown in Fig. 6. Porosity is varied by displacing alternate rods to form longitudinal slots as indicated in Fig. 7. A detailed description of the 2R wall is given in Ref. 5.

The original rod wall was built with the top of the rods tangent to the horizontal plane of the nozzle exit. Initial testing, Ref. 5, revealed that the resulting increase in tunnel cross-sectional area over the transition region (tunnel stations 1 to 4) produced an overexpansion at Mach numbers above 0.9. Therefore, the wall was modified to provide a constant tunnel cross-sectional area throughout the test section by extending the rods 0.029 in. into the airstream and contouring the transition region.

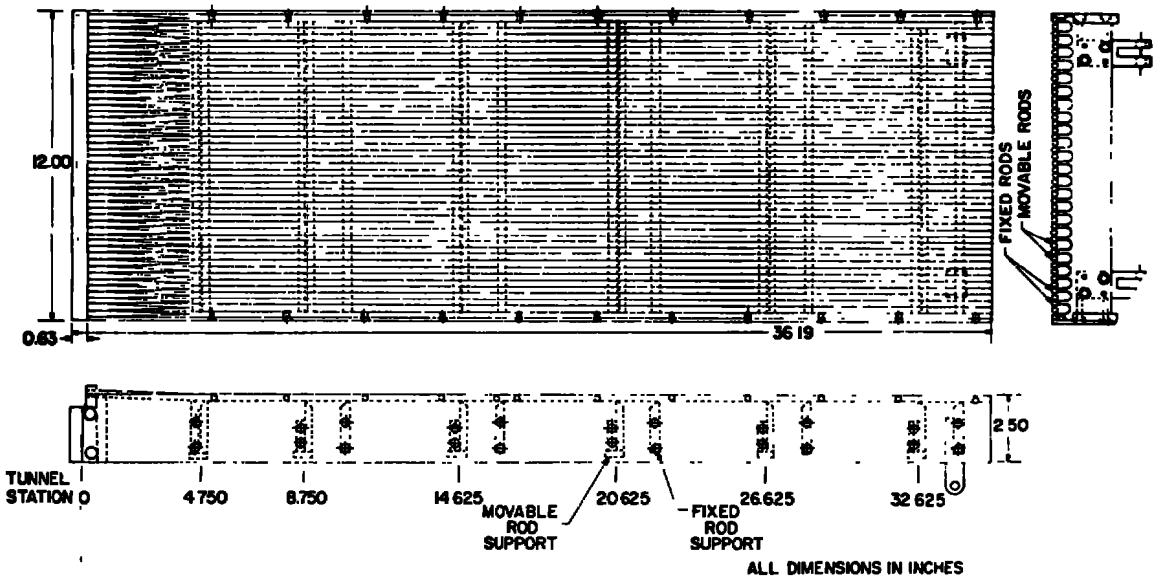

Figure 6. Detail of rod wall.

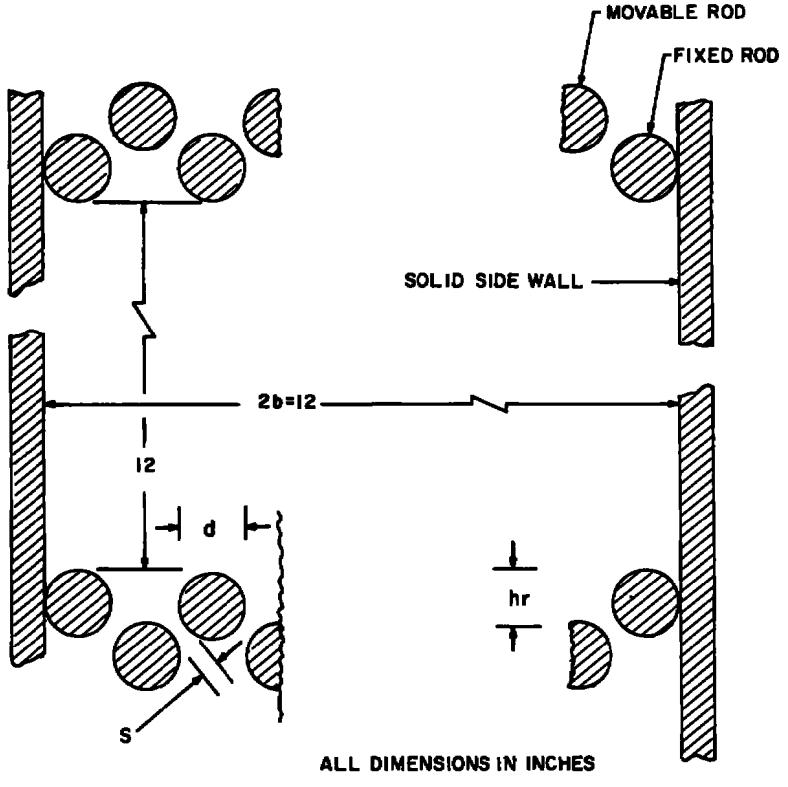

$$\tau = 100\left(\frac{ns}{2b}\right) = \frac{50n}{b}\left[(hr^2 + d^2)^{1/2} - d\right], \%$$

Figure 7. Cross section of rod wall.

2.2.4 Low-Noise Perforated Wall (LN)

The LN wall configuration is a modification of the standard Tunnel 1T P29 wall. The 6-percent nominal porosity wall consists of a 0.125-in.-thick plate with 0.125-in.-diam holes inclined to the airstream at an angle of 60 deg. The low-noise modification, which evolved from a study conducted in the Acoustic Research Tunnel, Ref. 6, consists of a 0.012-in.-thick splitter plate bisecting each hole longitudinally and extending half the depth of the hole. Figure 8 shows the LN wall configuration.

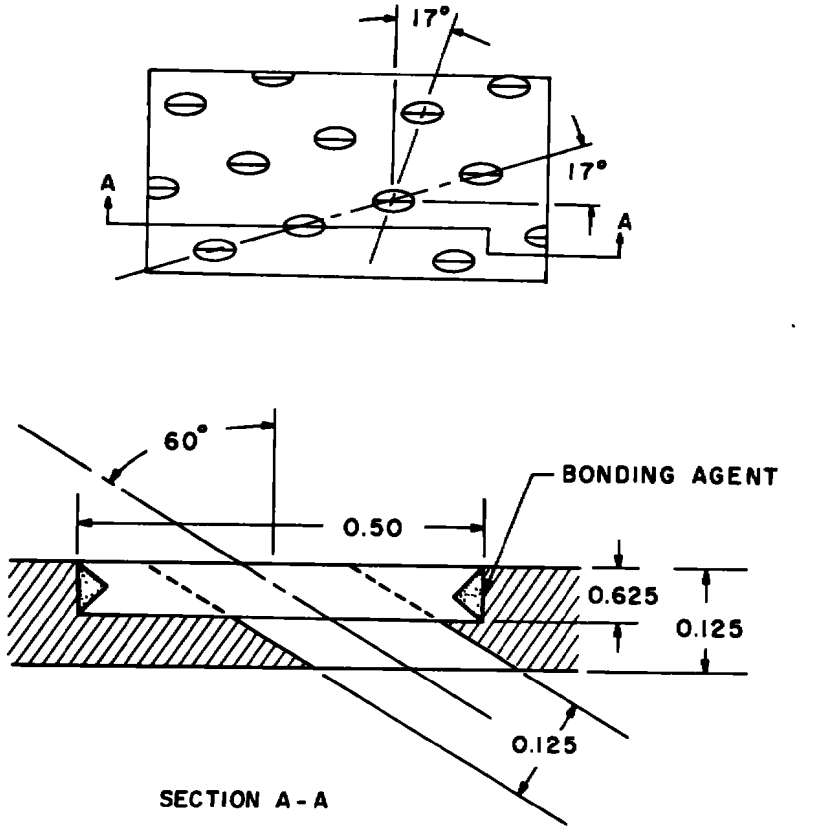

Figure 8. Details of low-noise perforated wall.

2.2.5 Slotted Wall (2S)

The 2S wall is based on a design suggested by personnel at the NASA-Langley Research Center. The wall configuration consists of six equally spaced slots in the top and bottom walls with solid side walls. Details of the slats and the variation of slot width along the test section are presented in Fig. 9. The maximum porosity of the 2S wall is 10 percent.

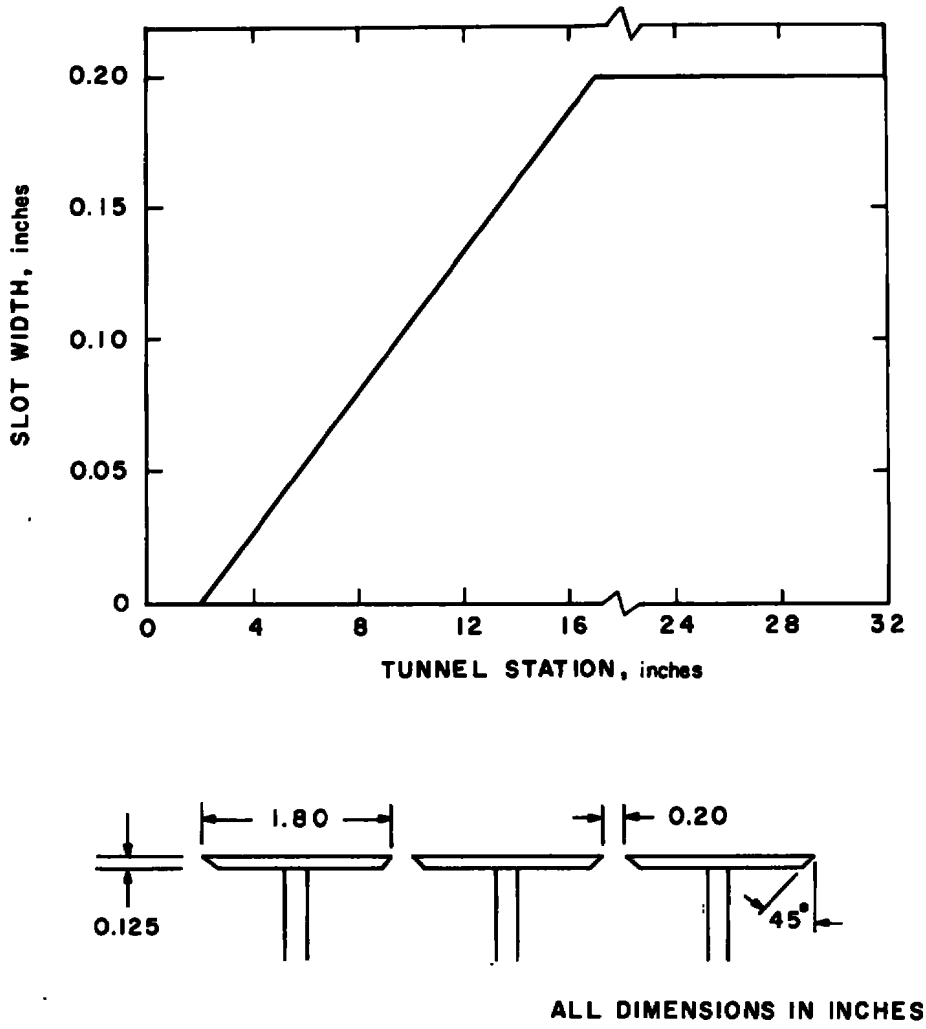

Figure 9. Details of slotted wall geometry.

2.3 STATIC PRESSURE PROBE

A 1-in.-diam static pressure probe was employed to obtain the centerline static pressure distribution from tunnel station -8.8 to 35.2. The probe has a total of 47 orifices spaced at 1-in. intervals along the probe. The probe attaches to the model support strut in the rear of the test section and is restrained by cables in the stilling chamber. The probe arrangement is shown in Fig. 10.

2.4 CONE-CYLINDER MODEL

A 20-deg, cone-cylinder model was used to investigate the influence of model blockage on the test section Mach number development. The 7-in.-long model was mounted

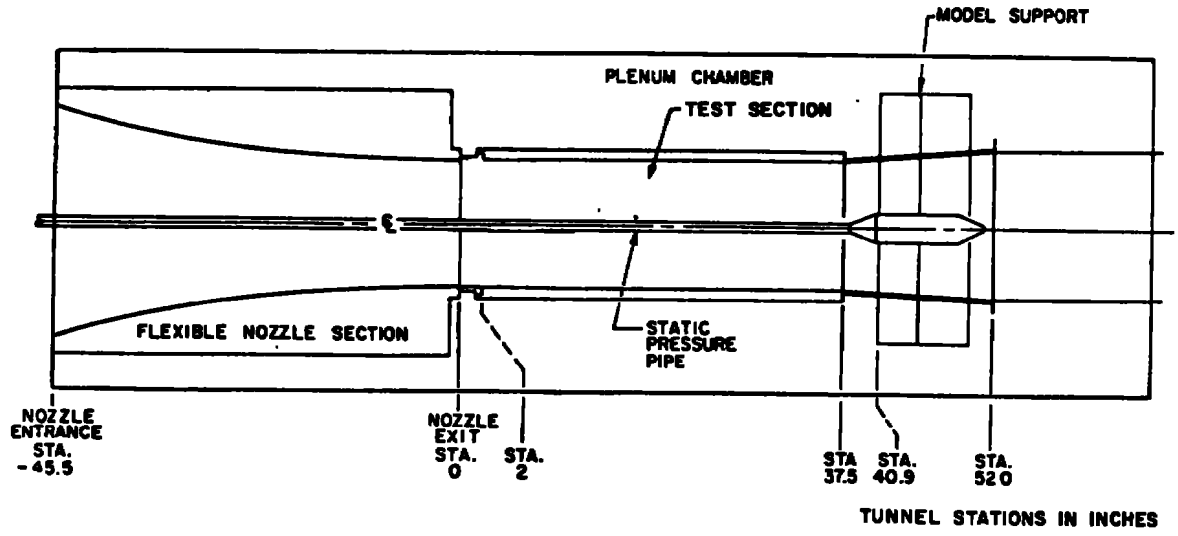

Figure 10. Centerline static probe test arrangement.

concentric with the centerline static probe, with the nose of the truncated cone located at station 12. The model blockage is 2.09 percent as computed by the ratio of the annular area of the cone-cylinder model as mounted on the static probe to the tunnel cross-sectional area less that of the static probe. Figure 11 shows the cone-cylinder model test arrangement.

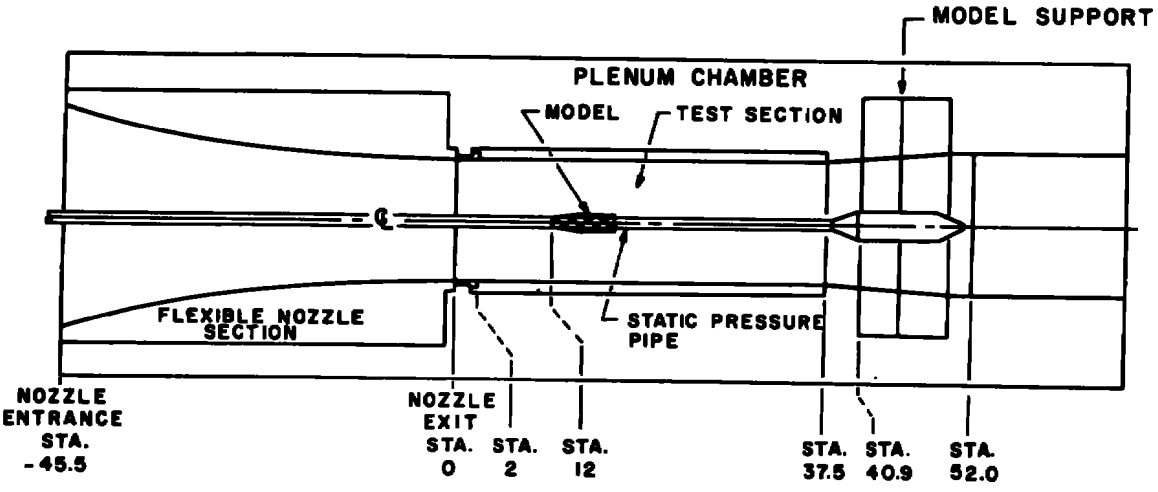

Figure 11. Cone-cylinder model test arrangement.

2.5 INSTRUMENTATION

Static pressure along the probe was measured by 15-psid strain-gage transducers. The plenum chamber reference pressure was measured with a servo-driven mercury manometer, and tunnel total pressure was measured by a precision pressure balance transducer. The tunnel total temperature was measured by an iron-constantan thermocouple. The instrumentation readings were recorded by an on-line computer system which reduced the raw data to engineering units, computed pertinent parameters, and tabulated the results.

3.0 TEST DESCRIPTION

3.1 TEST CONDITIONS

The tests were conducted at Mach numbers from 0.6 to 1.3. The stagnation pressure varied from 2750 to 2900 psfa, and the temperature was varied from 150 to 190°F. The porosity was varied from 2 to 7 percent for the LAR wall, from 3 to 8 percent for the ADP wall, and from 1 to 6 percent for the 2R wall. The LN wall porosity is nominally 6 percent, and the 2S wall maximum porosity is 10 percent. Table 1 summarizes the test conditions for each wall configuration.

Table 1. Summary of Test Conditions

Wall Configuration	Porosity, percent	Mach Number Range
LAR	7 (Full Open)	0.6 to 1.3
	2,3,5 (Cutoff Plate Upstream)	0.6 to 1.3
	2,3,5 (Cutoff Plate Downstream)	0.6 to 1.3
ADP	3,6,8 (Cutoff Plate Upstream)	0.6 to 1.3
2R	2,4,6	0.6 to 1.3
	1	0.8 to 1.1
LN	6	0.6 to 1.3
2S	10	0.6 to 1.3

3.2 PRECISION OF MEASUREMENTS

Uncertainties in the measurements were estimated from repeat calibrations of the instrumentation. The instrumentation uncertainties were then used to estimate uncertainties in other parameters using a Taylor series method of error propagation. The precision of the pertinent parameters is given in the following table:

ΔM	±0.002
TPR	±0.001
$\Delta p_c/p_t$	±0.001
$2\sigma M$	±0.0018
$\Delta\tau$(LAR)	±0.10
$\Delta\tau$(ADP)	±0.15
$\Delta\tau$(2R)	±0.25

4.0 RESULTS AND DISCUSSION

4.1 CALIBRATION PARAMETERS

The tunnel calibration yields a combination of tunnel pressure ratio, plenum chamber pressure, wall angle, and nozzle contour to provide a uniform test section Mach number distribution. Earlier calibration of the variable porosity wall (Ref. 7) showed that zero wall angle can be used rather than an optimum wall angle with a negligible increase in the centerline local Mach number deviation. Therefore, for the LAR, ADP, and LN wall configurations having four perforated walls, the wall angle was set at zero for the tunnel calibration at all Mach numbers. However, for the configurations with solid side walls, 2R and 2S, it was found necessary to diverge the walls to compensate for the side wall boundary-layer growth.

Supersonic Mach numbers can be generated in a partially open test section with a sonic nozzle and plenum suction. Expansion of the flow is achieved by removing air from the test section. For the calibrations reported herein, supersonic Mach numbers through 1.15 were generated in this manner with a resulting uniform Mach number distribution throughout the test region (tunnel stations 12 to 32). A specific converged-diverged nozzle contour was used to generate Mach numbers 1.2 and 1.3. Tables 2 through 6 present the values of tunnel pressure ratio, plenum chamber pressure ratio (p_c/p_t), wall angle (where applicable), and ΔM_c determined from the calibration of the five wall configurations.

Table 2. Calibration Data for LAR Wall

Porosity, percent	Mach Number	Pressure Ratio	p_c/p_t	ΔM
7 Full Open	0.60	1.09	0.797	0.017
	0.80	1.14	0.671	0.020
	0.90	1.16	0.608	0.024
	0.95	1.15	0.574	0.022
	1.00	1.20	0.545	0.025
	1.05	1.22	0.516	0.026
	1.10	1.29	0.484	0.028
	1.15	1.34	0.455	0.027
	1.20	1.39	0.430	0.031
	1.30	1.40	0.379	0.036
5 Cutoff Plate Upstream	0.60	1.08	0.791	0.011
	0.80	1.14	0.667	0.015
	0.90	1.25	0.604	0.022
	0.95	1.26	0.571	0.018
	1.00	1.26	0.539	0.019
	1.05	1.26	0.512	0.022
	1.10	1.27	0.480	0.025
	1.15	1.33	0.454	0.026
	1.20	1.33	0.427	0.024
	1.30	1.34	0.374	0.024
3 Cutoff Plate Upstream	0.60	1.08	0.788	0.004
	0.80	1.16	0.657	0.004
	0.90	1.16	0.593	0.000
	0.95	1.16	0.562	0.005
	1.00	1.16	0.531	0.002
	1.05	1.16	0.501	0.006
	1.10	1.28	0.469	0.002
	1.15	1.31	0.440	0.001
	1.20	1.32	0.411	-0.003
	1.30	1.34	0.357	-0.011
2 Cutoff Plate Upstream	0.60	1.08	0.778	-0.013
	0.80	1.11	0.654	-0.005
	0.90	1.23	0.591	-0.002
	0.95	1.22	0.558	-0.004
	1.00	1.32	0.526	-0.006
	1.05	1.32	0.494	-0.008
	1.10	1.32	0.463	-0.008
	1.15	1.32	0.434	-0.010
	1.20	1.32	0.409	-0.006
	1.30	1.34	0.355	-0.011

Table 2. Concluded

Porosity, percent	Mach Number	Pressure Ratio	p_c/p_t	ΔM
5 Cutoff Plate Downstream	0.60	1.11	0.798	0.025
	0.80	1.16	0.673	0.029
	0.90	1.16	0.608	0.031
	0.95	1.18	0.579	0.033
	1.00	1.21	0.548	0.035
	1.05	1.21	0.519	0.036
	1.10	1.21	0.460	0.038
	1.15	1.34	0.462	0.040
	1.20	1.34	0.434	0.040
	1.30	1.40	0.383	0.044
3 Cutoff Plate Downstream	0.60	1.11	0.799	0.027
	0.80	1.14	0.677	0.035
	0.90	1.16	0.617	0.038
	0.95	1.17	0.585	0.039
	1.00	1.19	0.556	0.042
	1.05	1.21	0.527	0.046
	1.10	1.28	0.497	0.048
	1.15	1.34	0.472	0.054
	1.20	1.40	0.442	0.052
	1.30	1.40	0.391	0.057
2 Cutoff Plate Downstream	0.60	1.10	0.803	0.027
	0.80	1.14	0.677	0.035
	0.90	1.15	0.616	0.039
	0.95	1.15	0.586	0.041
	1.00	1.20	0.555	0.045
	1.05	1.21	0.528	0.049
	1.10	1.28	0.500	0.049
	1.15	1.34	0.475	0.062
	1.20	1.41	0.444	0.057
	1.30	1.41	0.400	0.071

Table 3. Calibration Data for ADP Wall

Porosity, percent	Mach Number	Pressure Ratio	p_c/p_t	ΔM
8 Cutoff Plate Upstream	0.60	1.08	0.789	0.007
	0.80	1.13	0.662	0.010
	0.90	1.16	0.598	0.011
	0.95	1.16	0.567	0.011
	1.00	1.21	0.535	0.011
	1.05	1.21	0.506	0.012
	1.10	1.29	0.475	0.013
	1.15	1.35	0.448	0.015
	1.20	1.39	0.420	0.014
	1.30	1.40	0.368	0.013
6 Cutoff Plate Upstream	0.60	1.07	0.788	0.006
	0.80	1.15	0.662	0.008
	0.90	1.16	0.597	0.009
	0.95	1.16	0.565	0.010
	1.00	1.24	0.535	0.010
	1.05	1.21	0.504	0.011
	1.10	1.29	0.475	0.011
	1.15	1.35	0.449	0.013
	1.20	1.40	0.421	0.019
	1.30	1.40	0.369	0.019
3 Cutoff Plate Upstream	0.60	1.07	0.788	0.005
	0.80	1.14	0.662	0.007
	0.90	1.16	0.596	0.006
	0.95	1.16	0.564	0.007
	1.00	1.21	0.534	0.008
	1.05	1.21	0.504	0.008
	1.10	1.29	0.474	0.009
	1.15	1.39	0.445	0.010
	1.20	1.40	0.422	0.016
	1.30	1.40	0.369	0.017

Table 4. Calibration Data for 2R Wall

Porosity, percent	Mach Number	Wall* Angle	Pressure Ratio	p_c/p_t	Δ M
6	0.60	0	1.06	0.786	0.002
	0.80	↓	1.15	0.659	0.001
	0.90		1.17	0.591	0.000
	0.95		1.15	0.560	0.000
	1.00		1.16	0.529	0.000
	1.05		1.22	0.499	-0.001
	1.10		1.28	0.467	-0.001
	1.15		1.35	0.439	-0.004
	1.20		1.40	0.413	0.000
	1.30		1.41	0.360	-0.002
4	0.60	0	1.07	0.785	0.001
	0.80	↓	1.14	0.658	0.001
	0.90		1.16	0.592	0.000
	0.95		1.16	0.561	0.000
	1.00		1.17	0.527	0.000
	1.05		1.21	0.496	0.000
	1.10		1.28	0.468	-0.001
	1.20		1.40	0.411	0.000
	1.30		1.40	0.360	-0.002
2	0.60	0	1.07	0.787	0.002
	0.80	↓	1.14	0.658	0.002
	0.90		1.16	0.592	0.000
	0.95		1.16	0.559	-0.001
	1.00		1.16	0.526	-0.001
	1.05	↓	1.21	0.497	-0.002
	1.10	10	1.28	0.469	0.003
	1.20	10	1.39	0.413	0.004
	1.30	10	1.40	0.360	0.000
1	0.80	10	1.12	0.659	0.004
	0.90	↓	1.16	0.593	0.005
	0.95		1.16	0.562	0.006
	1.00		1.16	0.531	0.005
	1.05		1.21	0.500	0.004
	1.10		1.28	0.470	0.002

* Positive Angle for Diverged Wall

Table 5. Calibration Data for LN Wall

Mach Number	Pressure Ratio	P_c / p_t	ΔM
0.60	1.08	0.793	0.014
0.80	1.14	0.667	0.017
0.90	1.16	0.604	0.018
0.95	1.16	0.571	0.019
1.00	1.204	0.541	0.020
1.05	1.210	0.509	0.020
1.10	1.285	0.481	0.020
1.15	1.350	0.451	0.018
1.20	Maximum	0.423	0.019
1.30	Maximum	0.367	0.013

Table 6. Calibration Data for 2S Wall

Mach Number	Wall Angle, min	Pressure Ratio	p_c/p_t	ΔM
0.60	0	1.08	0.782	-0.003
0.80	20	1.14	0.653	-0.003
0.90	30	1.16	0.589	-0.002
0.95	18	1.16	0.558	-0.005
1.00	5	1.204	0.523	-0.008
1.05	5	1.210	0.494	-0.008
1.10	5	1.285	0.465	-0.007
1.20	5	Maximum	0.411	-0.007
1.30	10	Maximum	0.356	-0.009

4.2 CENTERLINE MACH NUMBER DISTRIBUTION

A quantitative evaluation of the Mach number distribution has been made by employing the standard deviation, σ, as an indication of the local deviation from the average free-stream Mach number in the test region. A value of $\pm 2\sigma$, computed for each distribution, is compared in the figures discussed below to the 2σ deviation for the standard Tunnel 1T 6-percent porosity, 60-deg-inclined-hole wall (P29) from Ref. 8.

During the test, an overexpansion near the nozzle exit was experienced for supersonic Mach numbers 1.2 and 1.3. which were generated with a contoured nozzle. The overexpansion occurred with all wall configurations and appears to be caused by a slight increase in the tunnel cross-sectional area in the region of the nozzle flexure (stations -4 to 0). The disturbance was progagated downstream and caused relatively high values of 2σ Mach number deviation at Mach numbers 1.2 and 1.3.

4.2.1 Low-Aspect-Ratio-Hole Wall (LAR)

Figures 12a through d present the centerline Mach number distribution, and Fig. 13a presents the 2σ Mach number deviation for the LAR wall with upstream cutoff plate displacement. For all porosities at subsonic Mach numbers, the centerline Mach number distribution is uniform and the 2σ Mach number deviation is as good or better than that for the standard Tunnel 1T P29 wall. At Mach numbers from 1.05 to 1.15 the Mach number deviation for the LAR wall (Fig. 13a) is larger than that for the P29 wall because of a disturbance originating in the solid to porous wall transition region (stations 2 to 10). Modification of the transition region would probably improve the distribution.

Centerline Mach number distribution and the 2σ Mach number deviation for the LAR wall with downstream cutoff plate displacement are shown in Figs. 12e through g and 13b, respectively. Downstream cutoff plate displacement caused an instability in the tunnel flow at all porosities with a corresponding increase in the Mach number deviation. A similar effect with downstream cutoff plate displacement was observed for the variable porosity wall in Tunnel 4T (Ref. 9). At lower values of porosity for the LAR wall with downstream cutoff plate displacement, fluctuations in the plenum chamber pressure up to ±30 psf were observed.

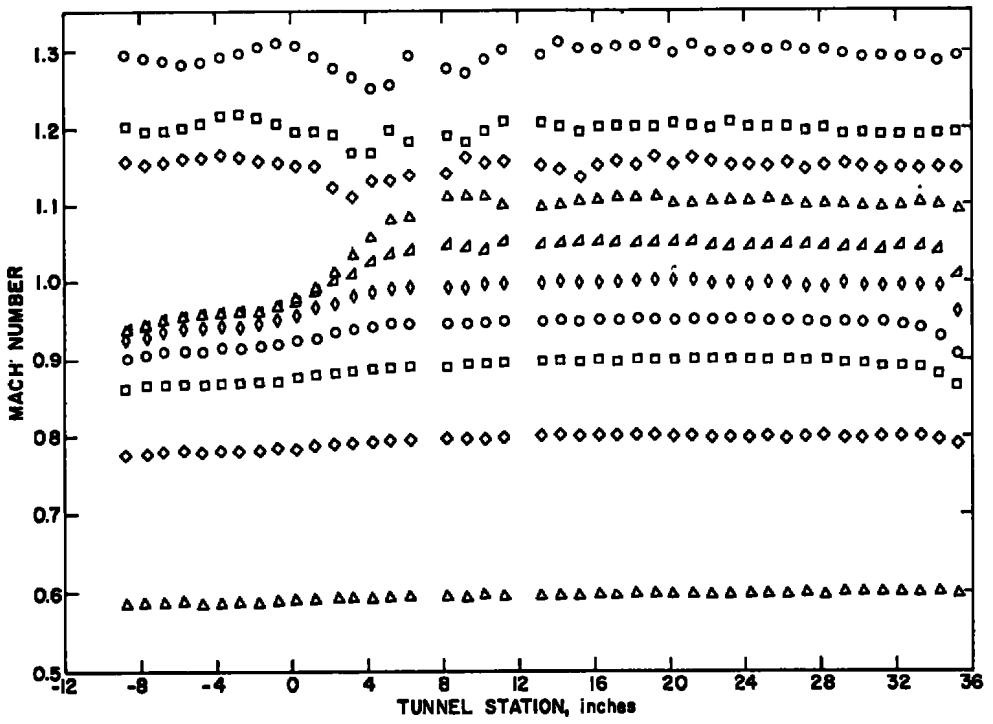

a. τ = 7 percent

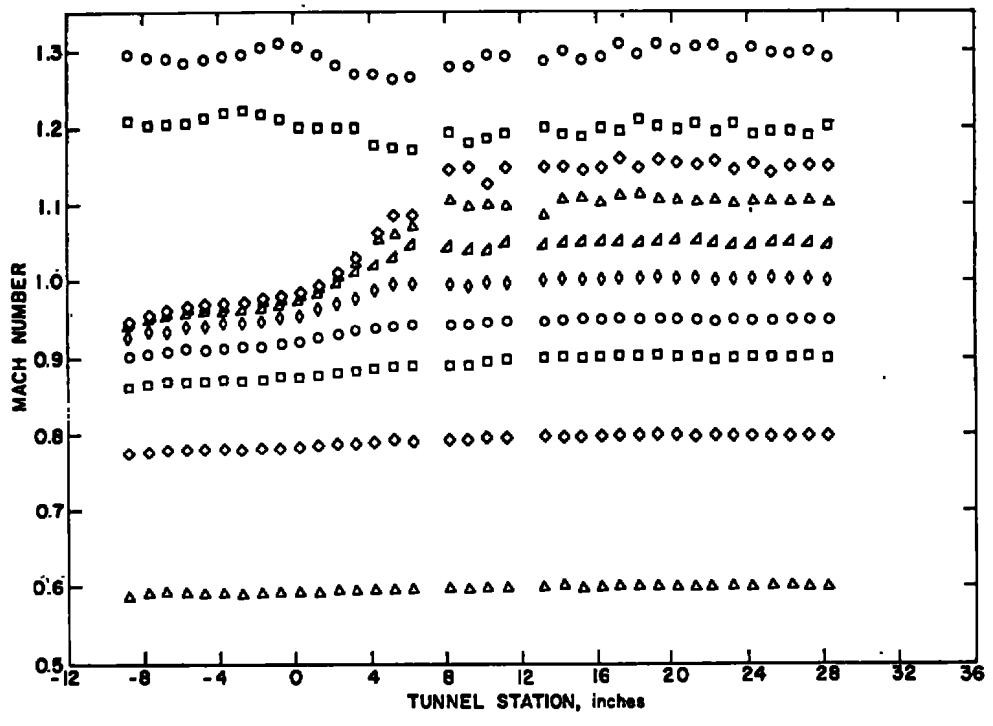

b. τ = 5 percent (cutoff plate upstream)

Figure 12. Centerline Mach number distribution, LAR wall.

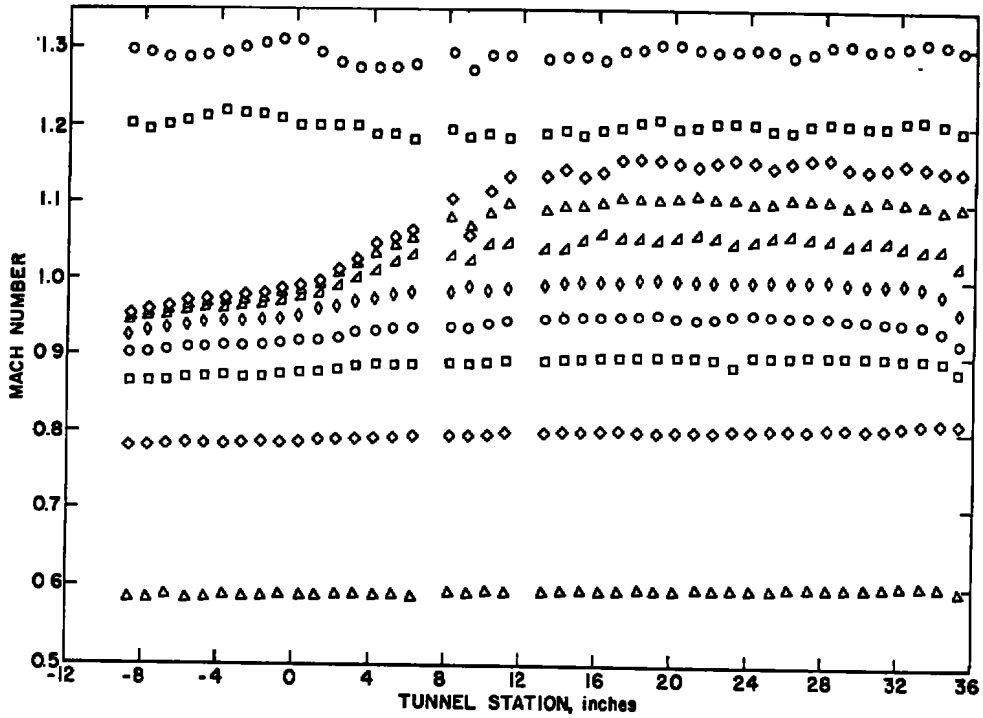

c. τ = 3 percent (cutoff plate upstream)

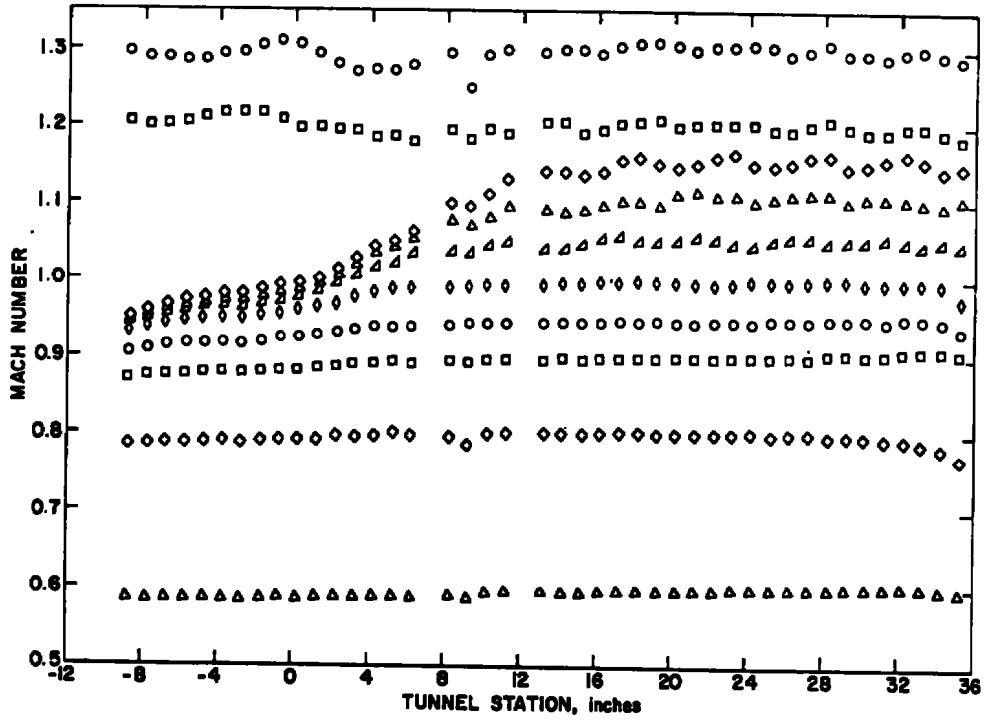

d. τ = 2 percent (cutoff plate upstream)

Figure 12. Continued.

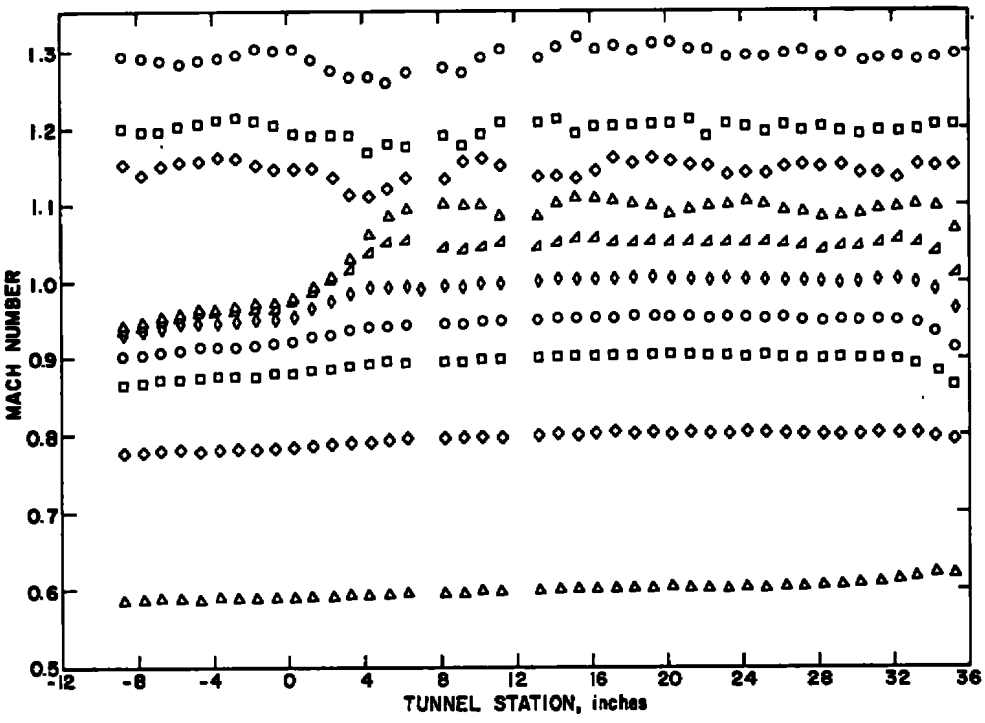

e. τ = 5 percent (cutoff plate downstream)

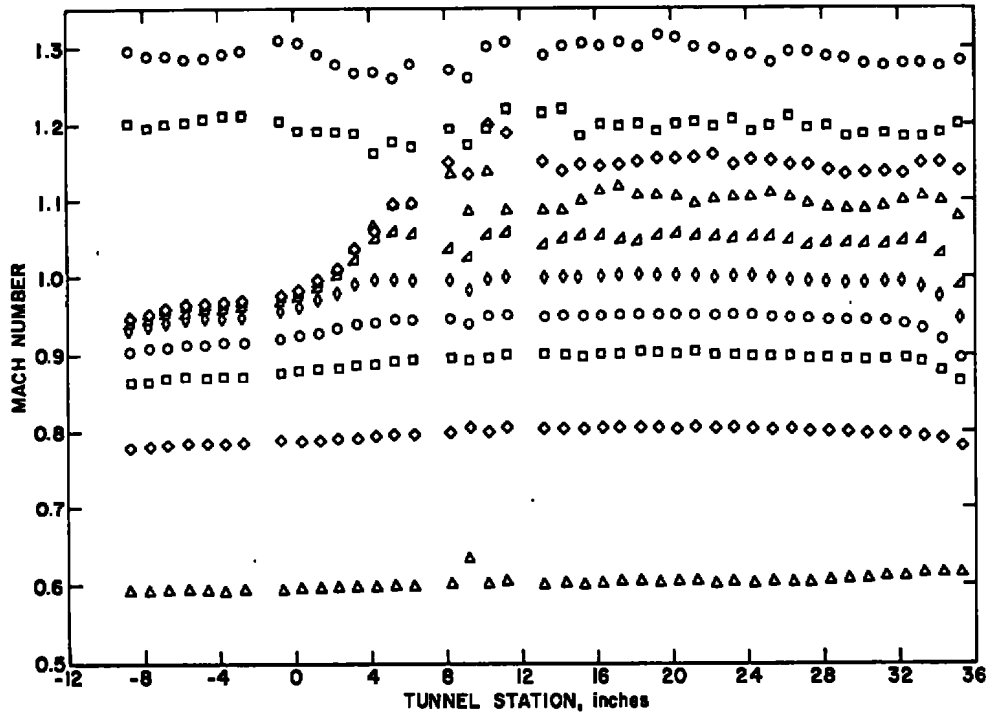

f. τ = 3 percent (cutoff plate downstream)

Figure 12. Continued.

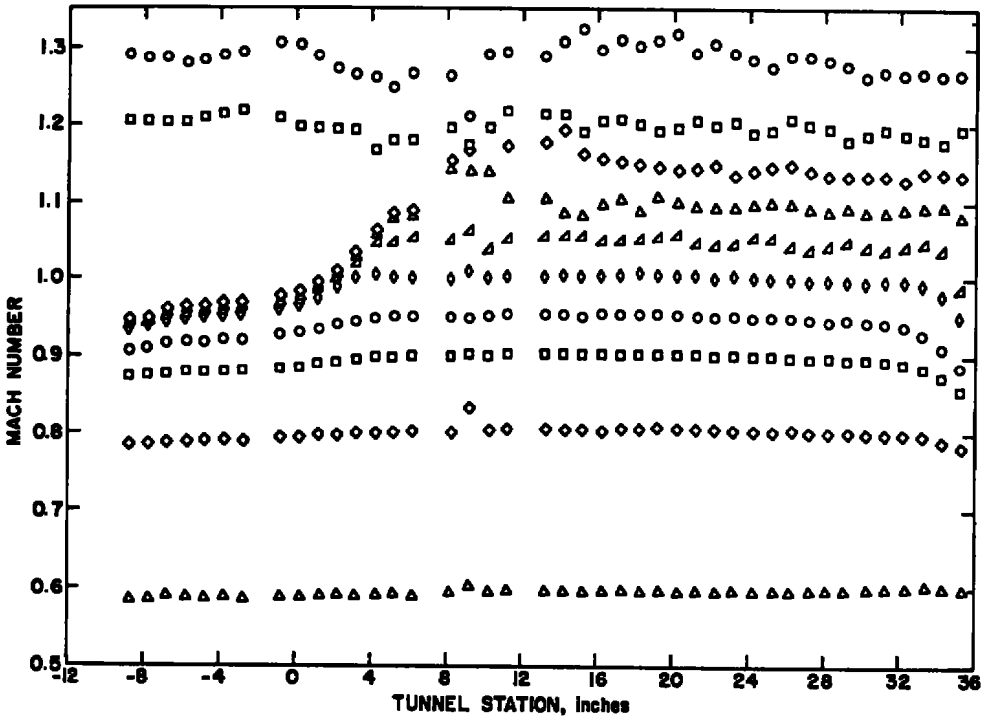

g. τ = 2 percent (cutoff plate downstream)
Figure 12. Concluded.

4.2.2 Axially Distributed Porosity Perforated Wall (ADP)

The centerline Mach number distribution and 2σ Mach number deviation for the ADP wall are presented in Figs. 14 and 15, respectively. Excellent Mach number distribution was obtained with the ADP wall for all porosities up to Mach number 1.2, where the nozzle flexure disturbance occurs. The 2σ Mach number deviation for the ADP wall is better than that of the P29 wall at Mach numbers below 1.1. The axial distribution of porosity effectively extends the solid to porous transition over a longer region of the test section than the other wall configurations. The smooth development of test section Mach number and the uniform Mach number distribution obtained with the ADP wall suggest that the Mach number distributions for other configurations may be improved by extending the transition region.

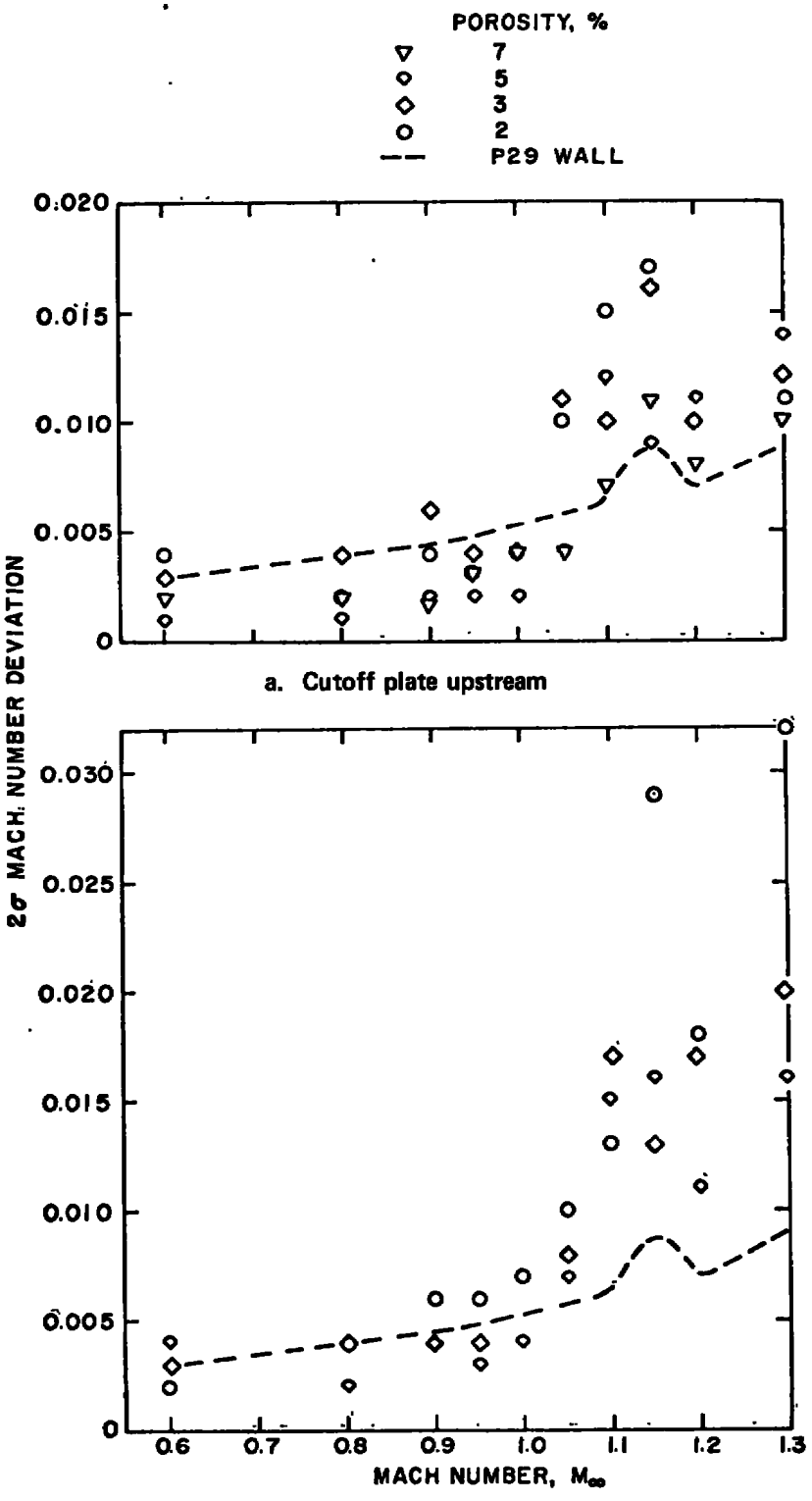

a. Cutoff plate upstream

b. Cutoff plate downstream

Figure 13. Local Mach number deviation, LAR wall.

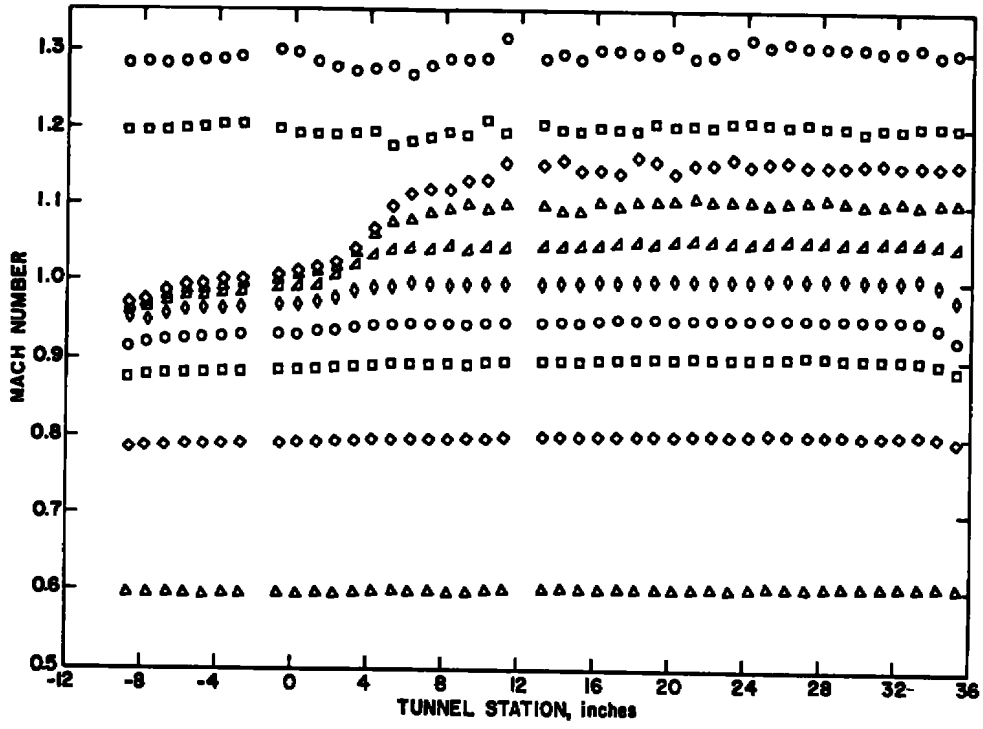

a. τ = 8 percent

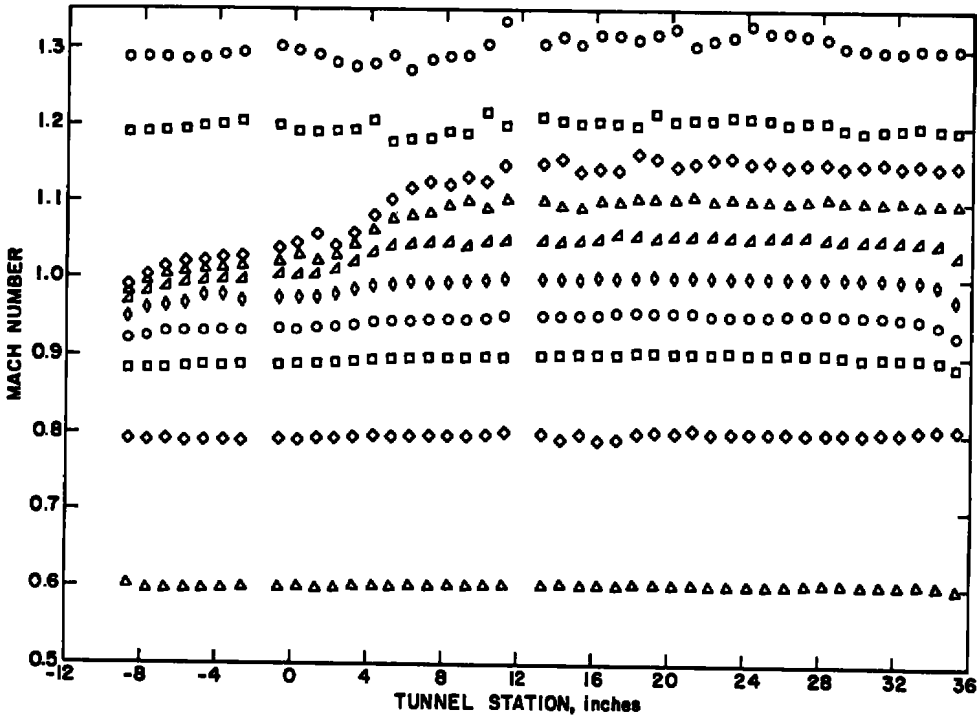

b. τ = 6 percent

Figure 14. Centerline Macn number distribution, ADP wall.

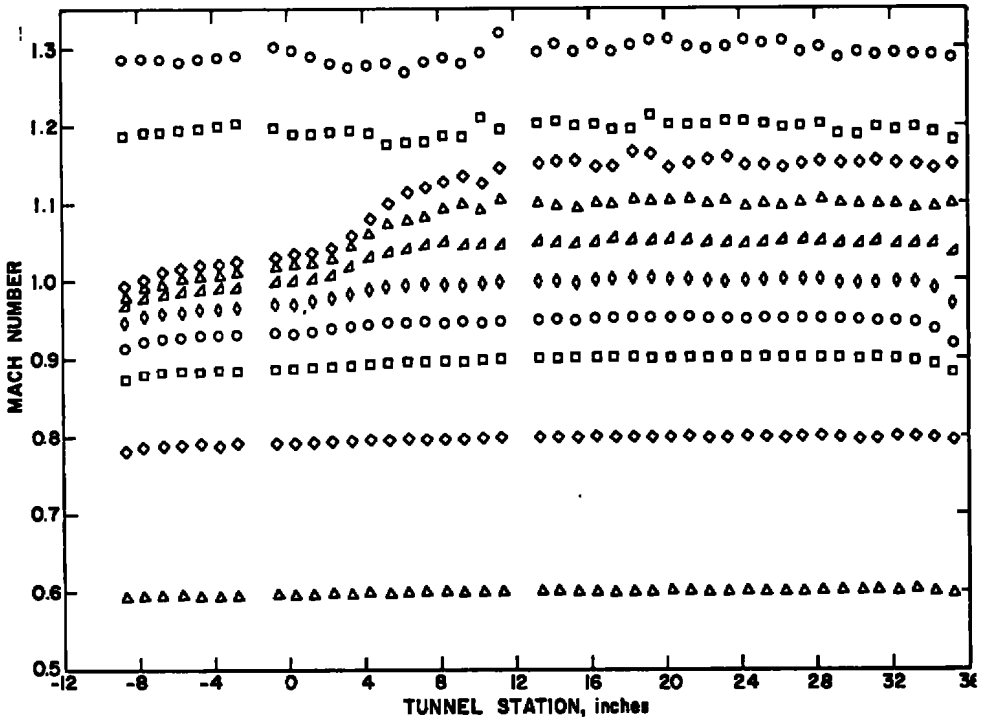

c. τ = 3 percent

Figure 14. Concluded.

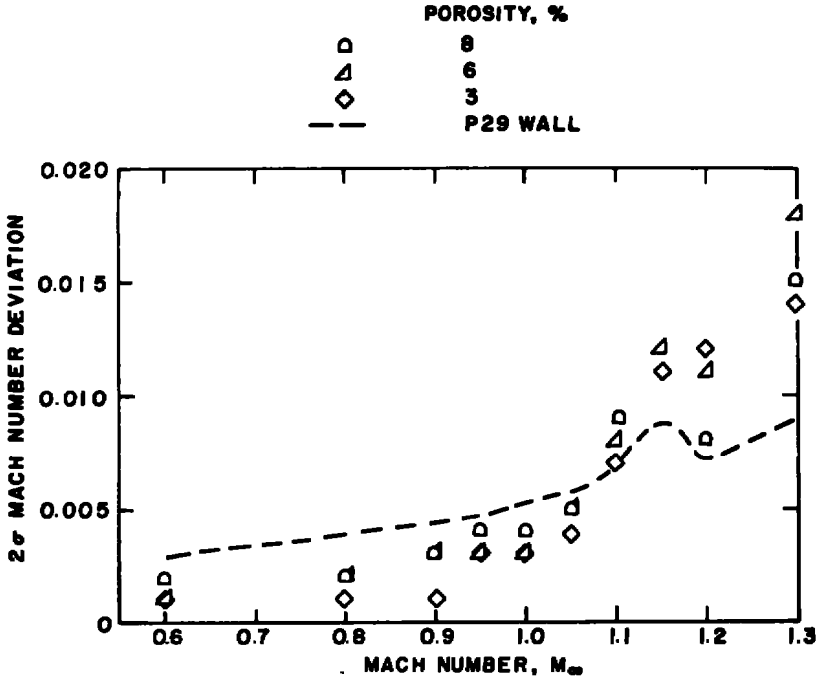

Figure 15. Local Mach number deviation, ADP wall.

4.2.3 Modified Rod Wall

The centerline Mach number distribution for the 2R wall is presented in Fig. 16. Figure 17 shows the 2σ Mach number deviation for the original and modified configurations. The modification to the transition region resulted in a significant improvement in the Mach number distribution for Mach numbers above 0.9 when compared to that of the original wall. The overexpansion at supersonic Mach numbers (Ref. 5) was essentially eliminated. The 2σ Mach number deviation for the 2R wall is equal to or less than that of the P29 wall up to Mach number 1.05 for 6-percent porosity and up to Mach number 1.2 for porosities of less than 6 percent. A uniform Mach number distribution can be obtained with a sonic nozzle contour for Mach numbers up to 1.2, whereas the original configuration required that a contoured nozzle be used to set Mach numbers between 1.05 and 1.2. Another significant improvement in the performance of the 2R wall by the transition modification is the elimination of the flow instability observed at 4-percent porosity for Mach numbers between 0.9 and 1.0 (Ref. 5). The top and bottom walls were diverged 10 min for Mach numbers above 1.05 for 2-percent porosity and for all Mach numbers for 1-percent porosity in order to compensate for the boundary-layer growth along the solid side walls.

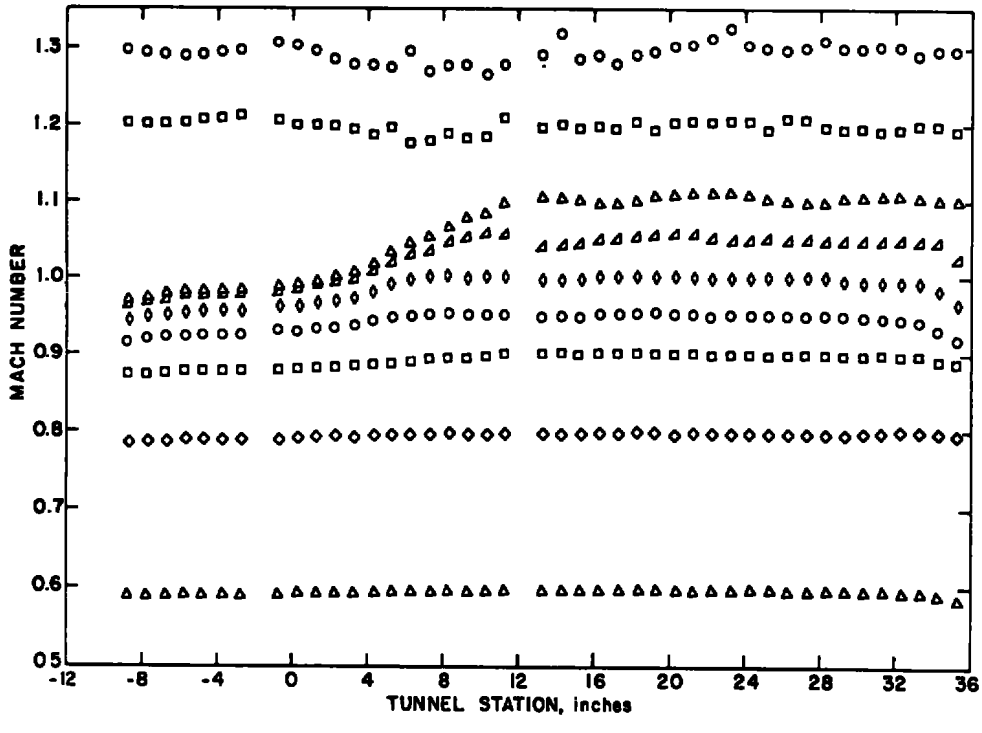

a. τ = 6 percent

Figure 16. Centerline Mach number distribution, 2R wall.

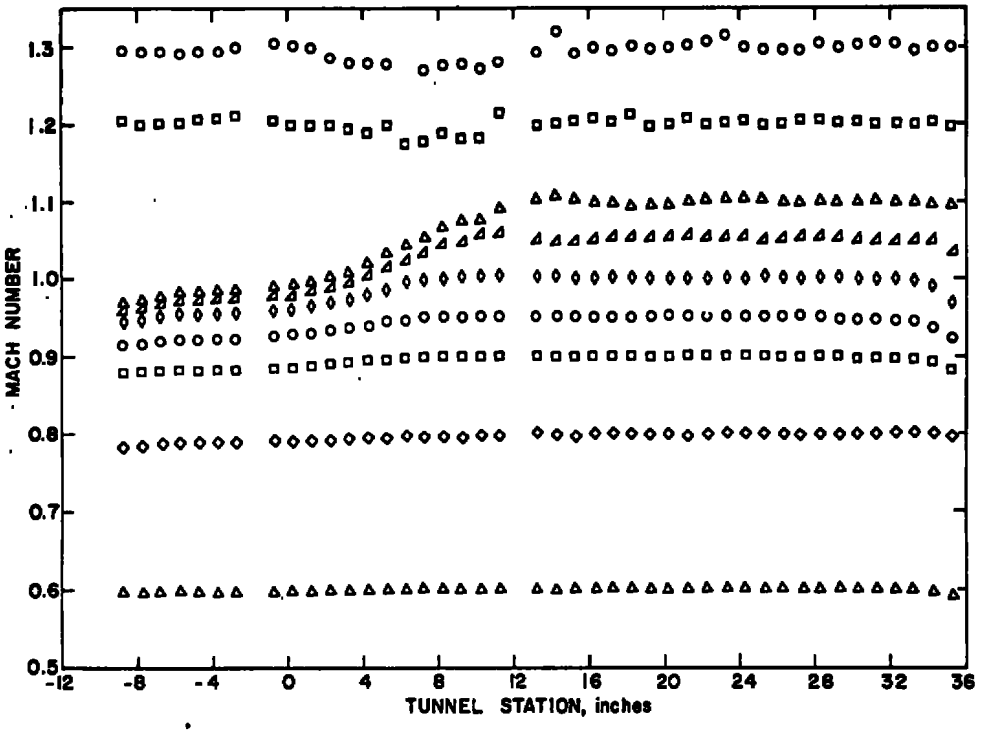

b. τ = 4 percent

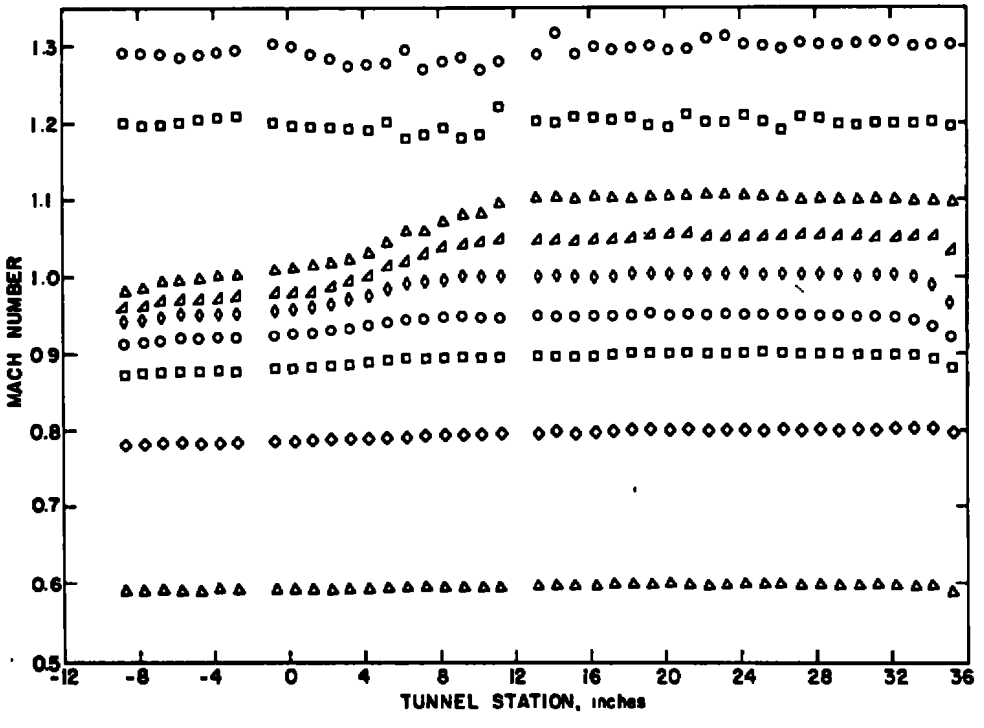

c. τ = 2 percent

Figure 16. Continued.

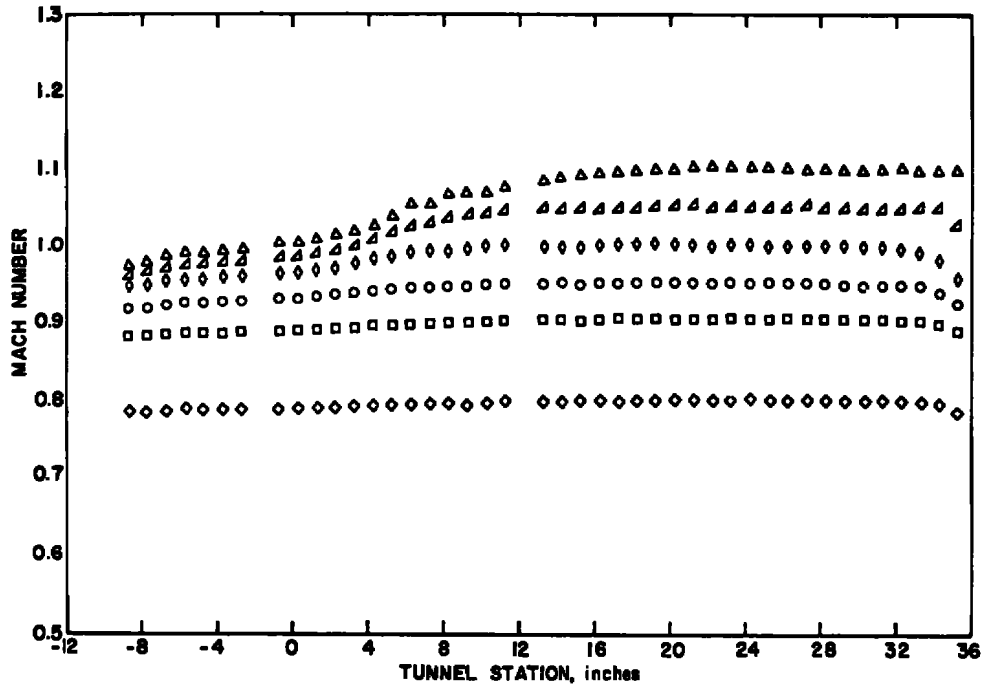

d. τ = 1 percent

Figure 16. Concluded.

4.2.4 Low-Noise Wall (LN)

Figures 18 and 19 show the centerline Mach number distribution and 2σ Mach number deviation, respectively, for the LN wall. The LN wall has a uniform centerline Mach number distribution with the 2σ Mach number deviation being less than or equal to that for the P29 wall for Mach numbers less than 1.1. At Mach numbers of 1.2 and 1.3, the LN wall Mach number deviation is greater than that of the P29 wall because of the nozzle flexure disturbance.

4.2.5 Slotted Wall (2S)

Figure 20 presents the centerline Mach number distribution, and Fig. 21 shows the 2σ Mach number number deviation for the 2S wall. A uniform centerline Mach number distribution is obtained with the 2S wall up to Mach number 1.1. At Mach numbers 1.2 and 1.3, the nozzle flexure disturbance propagates downstream through the test section with little attenuation. The 2σ Mach number deviation for the 2S wall is equal to or better than that for the P29 wall for the Mach number range from 0.6 to 1.1. It was necessary to diverge the top and bottom walls up to 30 min depending on the Mach number to compensate for the boundary-layer growth on the solid side walls. The wall angle schedule is shown in Table 6.

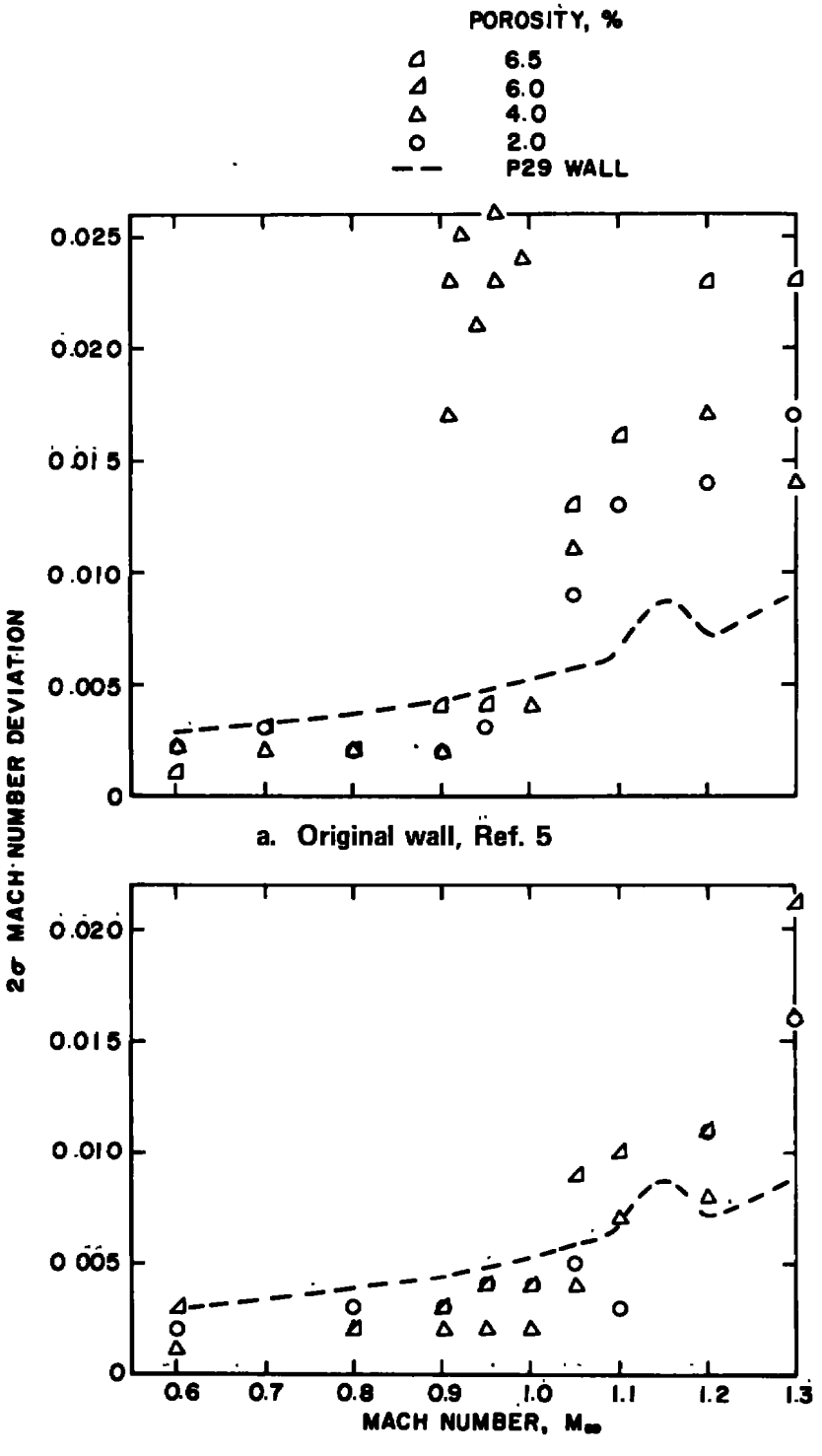

a. Original wall, Ref. 5

b. Modified wall

Figure 17. Local Mach number deviation, 2R wall.

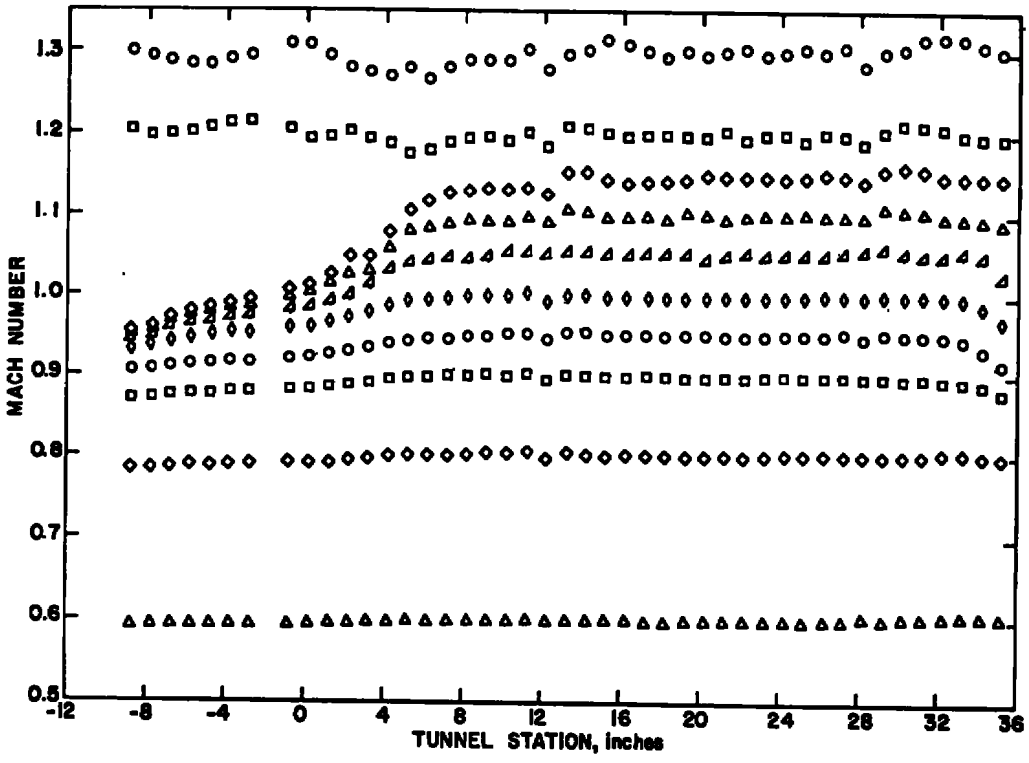

Figure 18. Centerline Mach number distribution, LN wall.

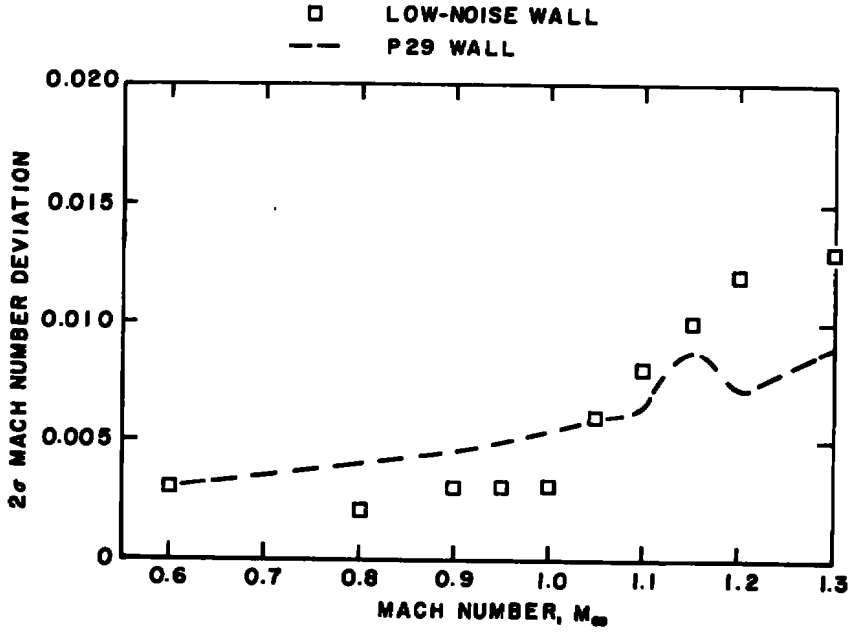

Figure 19. Local Mach number deviation, LN wall.

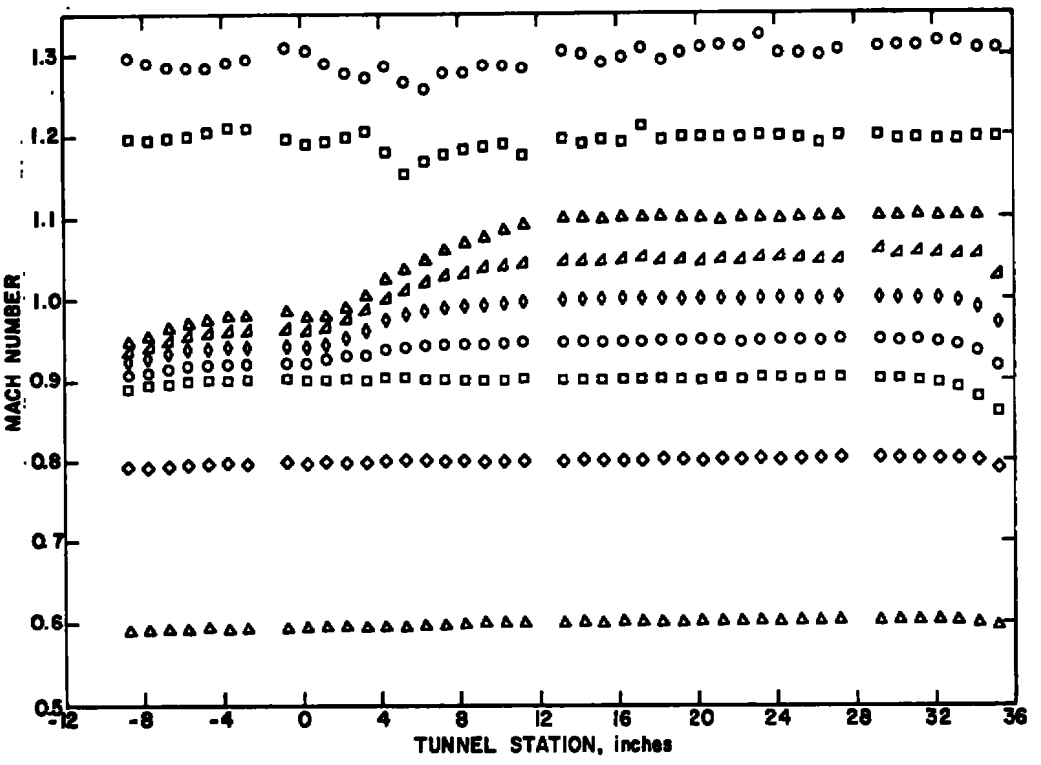

Figure 20. Centerline Mach number distribution, 2S wall.

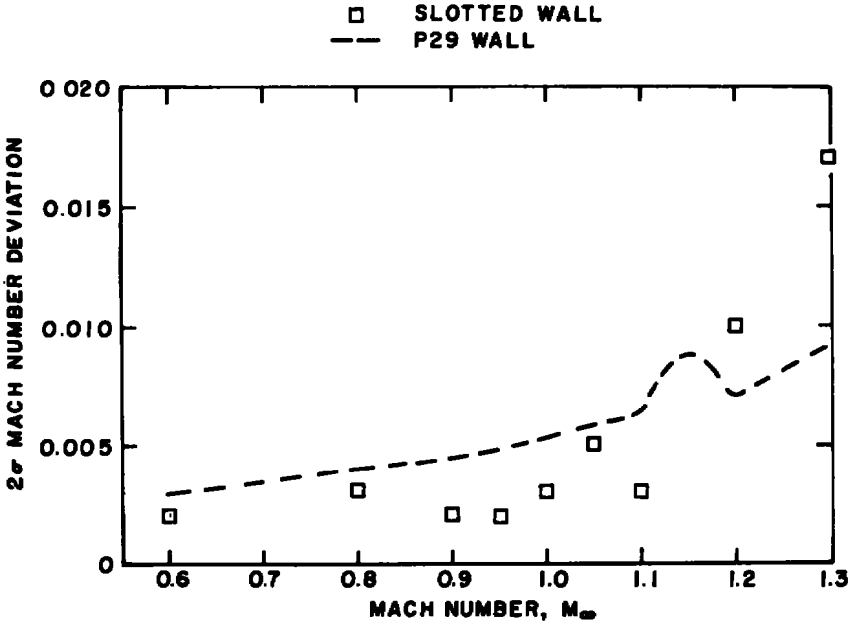

Figure 21. Local Mach number deviation, 2S wall.

4.3 MODEL BLOCKAGE EFFECTS ON THE CALIBRATION MACH NUMBER

The test section Mach number in the AEDC transonic wind tunnels, as in many others, is established by setting a pressure ratio, TPR, across the test section and the so-called plenum Mach number, M_c, as related through a tunnel-empty calibration to the average centerline Mach number in some specified test region. It is generally presumed that when the model size is small compared to the test section area the tunnel calibration Mach number is not affected by the presence of the model. However, as noted in Section 1.0, questions have arisen concerning the preciseness of the test section Mach number set with TPR and M_c. Thus, data were taken with a 2.09-percent blockage cone-cylinder model mounted concentric with the centerline probe. The effect of the model on the free-stream Mach number was determined from the average change in the nozzle Mach number distribution between stations -8.8 and -0.8 computed by the relation

$$M_{AVG} = \frac{\sum_{i=1}^{n} [(M_i - M_c)_m - (M_i - M_c)_o]}{n} \tag{3}$$

where the subscripts m and o denote model installed and tunnel empty, respectively. Figures 22 and 23 present the parameter ΔM_{AVG} for the wall configurations. Included in the figures is the average change of Mach number in the measurement region caused by the model in free air predicted by the Douglas-Neumann computer program, Ref. 10. For porosities greater than 3 percent with the configurations having four perforated walls, ΔM_{AVG} is zero within the accuracy of the measurement (Fig. 22). When the porosity is 3 percent or less, there is an effect of the model which increases with decreasing porosity. A much larger change in the Mach number in the nozzle can be seen with the 2R and 2S configurations (Fig. 23), both slotted wall configurations with solid side walls. A question arises as to whether the increased effect of blockage with the 2R and 2S wall is associated with the slotted wall design or the solid side walls, or both. The parameter ΔM_{AVG} for the Tunnel 4T-type variable porosity wall (see Fig. 4) with all four walls ventilated and with solid side walls is presented in Fig. 24. It is seen that the solid side walls do increase the effect of the model blockage on the calibration Mach number, which can explain, in part, the larger effects seen for the 2S and 2R walls. However, comparing Figs. 23 and 24, there appears to be an additional change in the calibration Mach number attributable to the slotted wall design. No attempt was made to investigate other means of setting the test section Mach number.

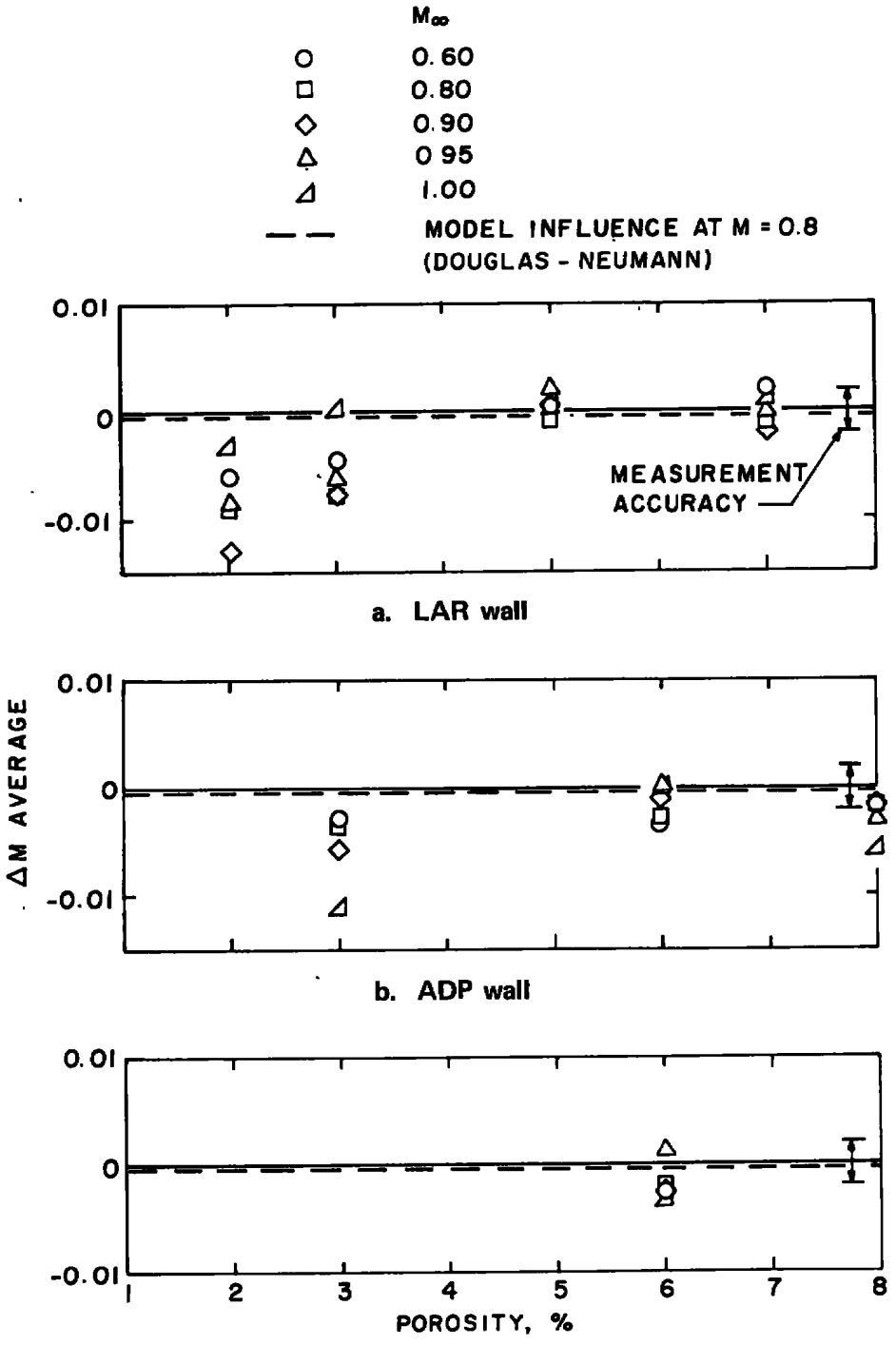

Figure 22. Blockage effect for perforated wall configurations.

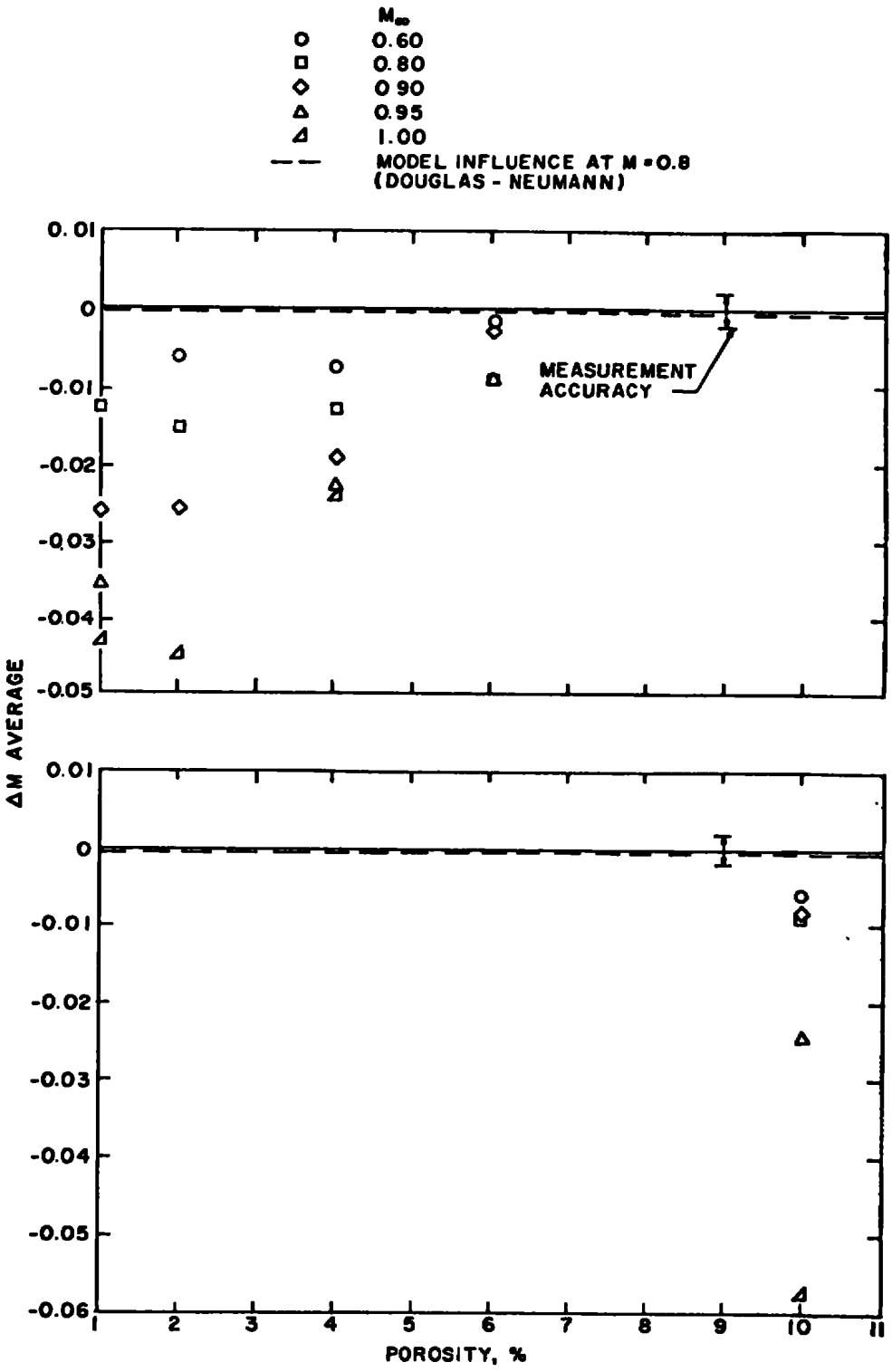

Figure 23. Blockage effect for slotted wall configurations.

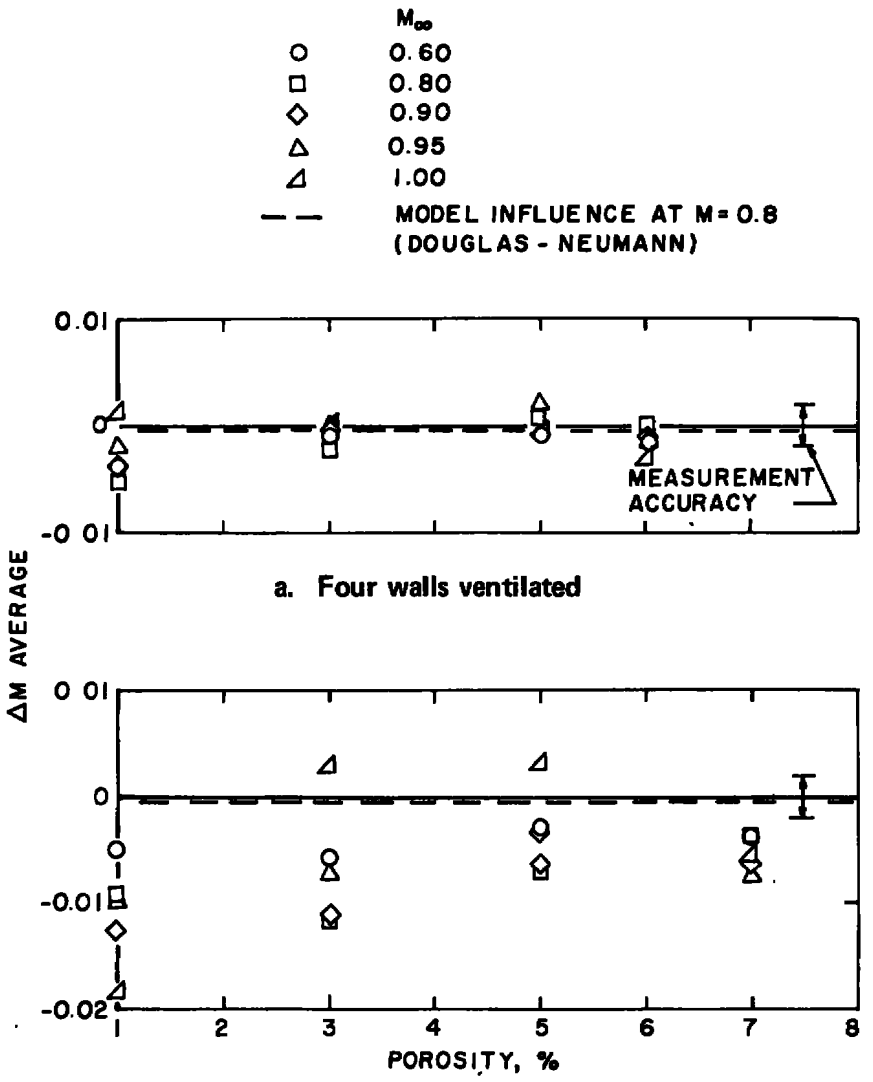

a. Four walls ventilated

b. Side walls solid

Figure 24. Influence of solid side walls on blockage effect for variable porosity wall.

Figures 25 through 29 show the distribution of ΔM, where ΔM is computed by the relation inside the brackets of Eq. (3), for the wall configurations with the cone-cylinder model installed around the centerline probe. Included for M = 0.8 is the theoretical model influence computed from the Douglas-Neuman free air solution. Data shown are for only one wall porosity for the variable porosity configurations and are typical of all porosities. The deviation of the data from free-stream conditions at the rear of the test section for the LAR, 2R, and 2S walls at Mach number 0.9 and the ADP wall at Mach number 0.8

were caused by operating the tunnel with an incorrect tunnel pressure ratio. With those exceptions, however, the data for all wall configurations show that the tunnel flow, perturbed by the model, returns to free-stream conditions at the end of the test section. The most interesting phenomenon depicted in Figs. 25 through 29 is that the above holds true even for the cases where a significant blockage effect appears upstream in the nozzle region. The mechanism responsible for these contradictory effects of model blockage is not yet fully understood.

5.0 CONCLUDING REMARKS

Tunnel calibration and centerline Mach number distribution were obtained in Tunnel 1T for a low-aspect-ratio-hole wall, an axially distributed porosity perforated wall, a rod wall, a low-noise perforated wall, and a slotted wall. Relatively uniform centerline Mach number distributions were obtained with all wall configurations with the exception of the LAR wall with downstream cutoff plate displacement, which also resulted in an instability in tunnel operation. Relatively large values of the 2σ Mach number deviation for all wall configurations at M = 1.2 and 1.3 are attributable to a disturbance generated at the tunnel nozzle flexure being propagated downstream through the test region.

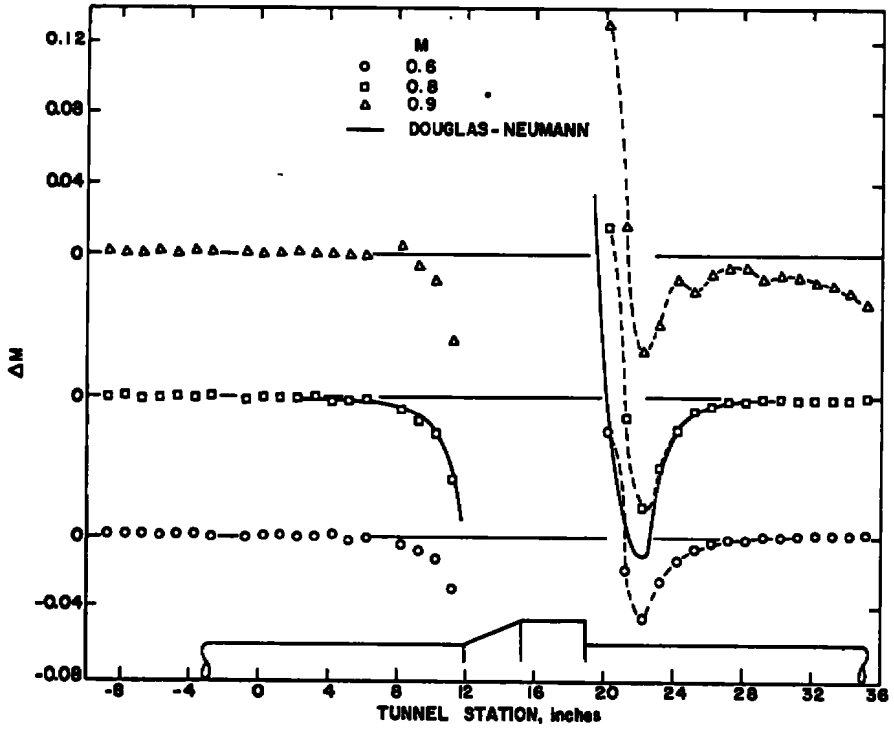

Figure 25. Centerline Mach number distribution with cone-cylinder, LAR wall (τ = 5 percent).

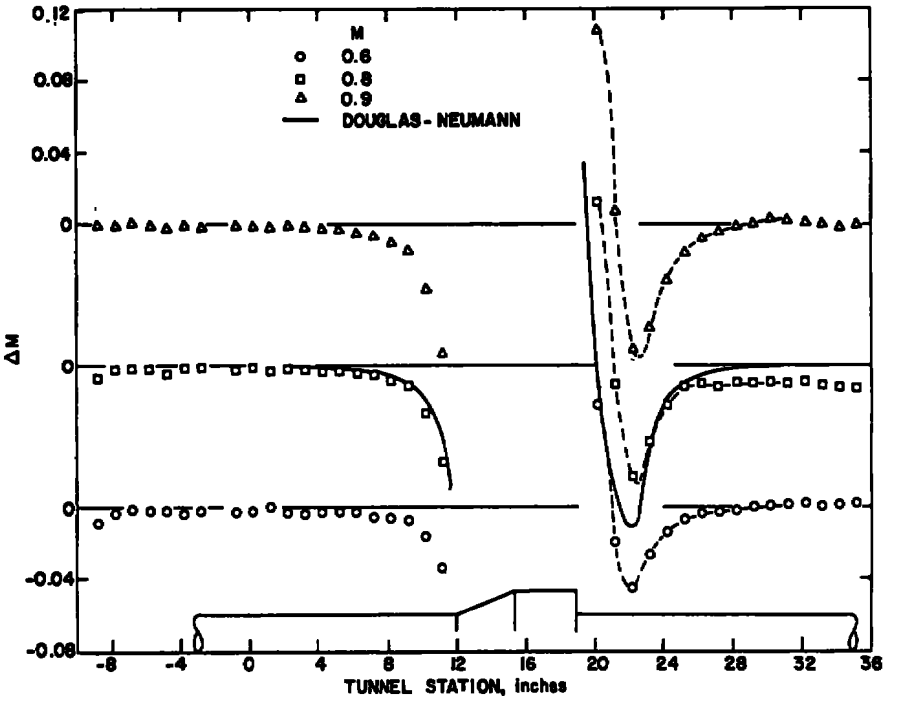

Figure 26. Centerline Mach number distribution with cone-cylinder, ADP wall (τ = 6 percent).

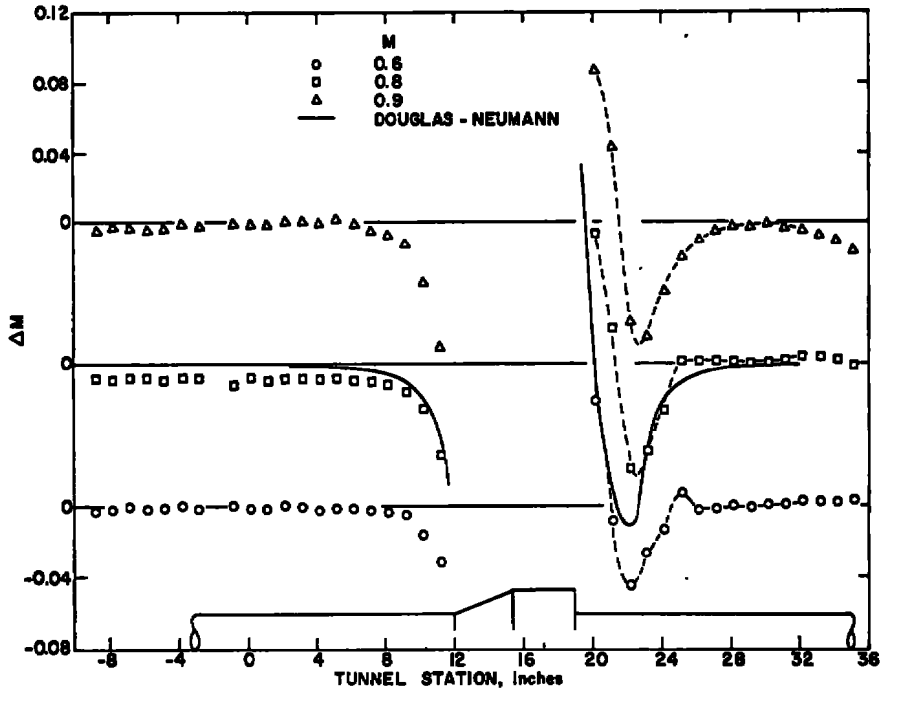

Figure 27. Centerline Mach number distribution with cone-cylinder, 2R wall (τ = 6 percent).

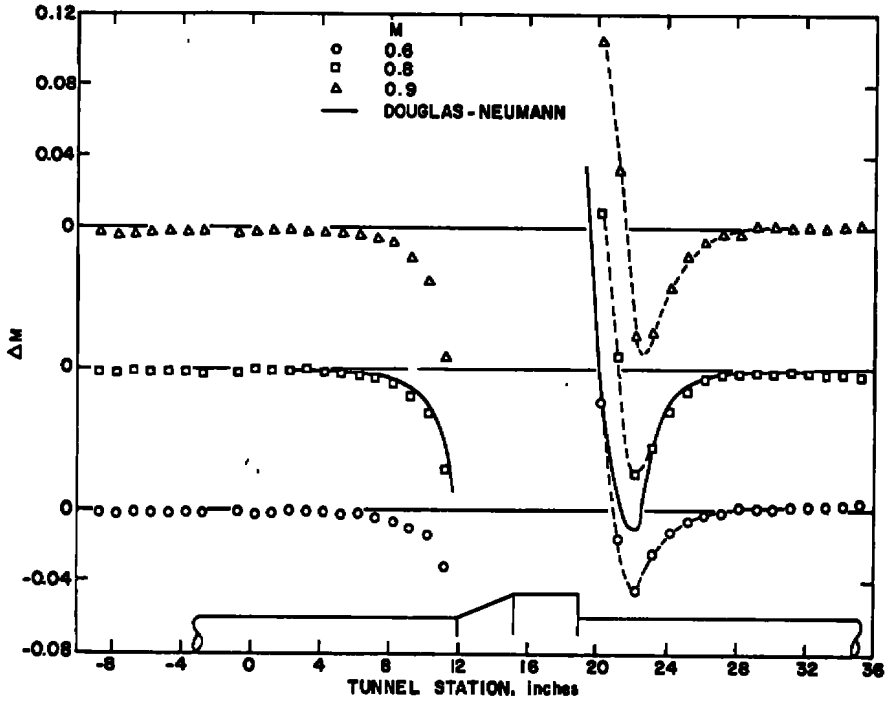

Figure 28. Centerline Mach number distribution with cone-cylinder, LN wall.

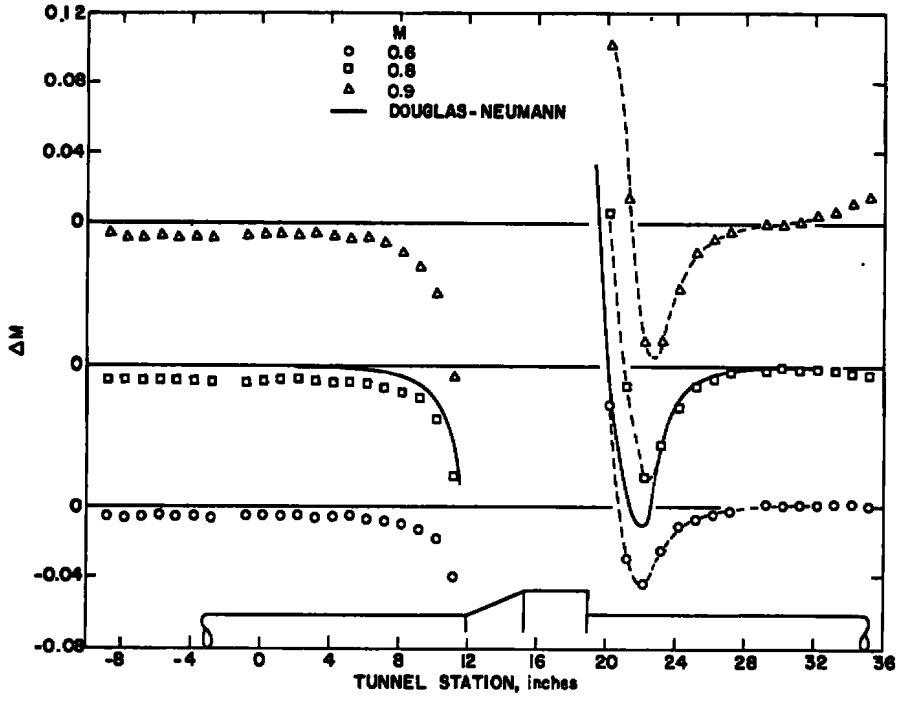

Figure 29. Centerline Mach number distribution with cone-cylinder, 2S wall.

The tunnel calibration Mach number is affected by the model blockage for the slotted wall configurations (2R and 2S) and for the perforated wall configurations (LAR and ADP) at wall porosities of 3 percent or less. It was found that the effect on the Mach number distribution upstream of the model is an undetermined function of Mach number, wall geometry, and porosity. However, no effects of model blockage were observed downstream of the model where the flow returned to the calibrated free-stream conditions at the end of the test section.

REFERENCES

1. Binion, T. W., Jr. "An Investigation of Three-Dimensional Wall Interference in a Variable Porosity Transonic Wind Tunnel." AEDC-TR-74-76 (AD787658), October 1974.

2. Jacocks, J. L. "Determination of Optimum Operating Parameters for the AEDC-PWT-4-Ft Transonic Tunnel with Variable Porosity Test Section Walls." AEDC-TR-69-164 (AD857045), August 1969.

3. Chew, W. L. "Cross-Flow Calibration at Transonic Speeds of Fourteen Perforated Plates with Round Holes and Airflow Parallel to the Plates." AEDC-TR-54-65 (AD69609), July 1955.

4. Binion, T. W., Jr. and Lo, C. F. "Application of Wall Corrections to Transonic Wind-Tunnel Data." AIAA Paper No. 72-1009, AIAA 7th Aerodynamic Testing Conference, Palo Alto, California, September 13-15, 1972.

5. Binion, T. W., Jr. and Anderson, C. F. "An Experimental Investigation of the Acoustic and Wall Interference Properties of Rod and Perforated Wind Tunnel Walls in Two-Dimensional Transonic Flow." AEDC-TR-74-41 (AD922394L), September 1974.

6. Dougherty, N. S., Anderson, C. F., and Parker, R. L., Jr. "An Experimental Investigation of Techniques to Suppress Edgetones from Perforated Wind Tunnel Walls." AEDC-TR-75-88, August 1975.

7. Jackson, F. M. "Calibration of the AEDC-PWT 1-Ft Transonic Tunnel with Variable Porosity Test Section Walls." AEDC-TR-69-114 (AD853073), May 1969.

8. Jackson, F. M. and Sloan, E. H. "Calibration of the AEDC-PWT 1-Foot Transonic Tunnel." AEDC-TR-68-4 (AD827912), February 1968.

9. Hartley, M. S. and Jacocks, J. L. "Initial Calibration Results from the AEDC-PWT 4-Foot Transonic Tunnel." AEDC-TR-68-141 (AD837078), August 1968.

10. Smith, A. M. O. and Pierce, Jesse. "Exact Solution of the Neumann Problem, Calculation of Non-Circulatory Plane and Axially Symmetric Flows About or Within Arbitrary Boundaries." Douglas Aircraft Company Report No. ES 26988, April 1958.

NOMENCLATURE

A	Cutoff plate displacement, in.
ADP	Axially distributed porosity perforated wall
b	Tunnel semiwidth, in.
C_P	Pressure coefficient at the wall, $(p - p_\infty)/q_\infty$
D	Porous wall hole diameter, in.
d	Rod diameter, in., see Fig. 7
h	Tunnel semiheight, ft
hr	Rod displacement measured normal to wall, in., see Fig. 7
L	Axial distance between holes, in.
LAR	Low-aspect-ratio-hole wall
LN	Low-noise perforated wall
M	Mach number
M_c	Equivalent plenum Mach number
M_∞	Free-stream Mach number
ΔM_{AVG}	Model blockage effect parameter, see Eq. (3)
ΔM_c	Mach number calibration parameter, $M_\infty - M_c$
n	Number of slots, see Fig. 7
p_c	Plenum chamber static pressure, psfa

p_e	Diffuser exit static pressure, psfa
p_t	Stilling chamber total pressure, psfa
p_∞	Free-stream static pressure, psfa
Q	Porosity parameter, $(1 + \beta/R)^{-1}$
q_∞	Free-stream dynamic pressure, psf
R	Porosity factor, $2\theta/C_P$
2R	Rod wall
2S	Slotted wall
S	Slot width, in.
TPR	Tunnel pressure ratio, p_t/p_e
X	Tunnel station, in.
β	Compressibility factor, $\sqrt{1 - M_\infty^2}$
θ	Stream flow angle at the wall, deg
θw	Test section wall angle, deg (positive diverged)
λ	Tunnel height-to-width ratio, h/b
σ	Standard deviation
τ	Test section wall porosity, percent